Sources of organic aerosols in eastern China: A modeling study with high-resolution intermediate-volatility and semi-volatile organic compound emissions

Jingyu An[1], Cheng Huang[1*], Dandan Huang[1], Momei Qin[2,1], Huan Liu[3], Rusha Yan[1], Liping Qiao[1], Min Zhou[1], Yingjie Li[1], Shuhui Zhu[1], Qian Wang[1], Hongli Wang[1]

1. State Environmental Protection Key Laboratory of the Formation and Prevention of Urban Air Pollution Complex, Shanghai Academy of Environmental Sciences, Shanghai 200233, China

2. Jiangsu Key Laboratory of Atmospheric Environment Monitoring and Pollution Control, Collaborative Innovation Center of Atmospheric Environment and Equipment Technology, Nanjing University of Information Science & Technology, Nanjing 210044, China

3. State Key Joint Laboratory of Environment Simulation and Pollution Control, School of Environment, Tsinghua University, Beijing 100084, China

Abstract: Current chemical transport models fail to reproduce both the concentrations and temporal variations of Organic aerosol (OA), especially the secondary organic aerosol (SOA), hindering the identification of major contribution sources. The absence of precursors, especially intermediate-volatility and semi-volatile organic compounds (I/SVOCs), has a significant impact on the performance of SOA simulation. Herein, we established a high-resolution emission inventory of I/SVOCs and by incorporating it into the CMAQ model, concentrations, temporal variations, and spatial distributions of POA and SOA originated from different sources in the Yangtze River Delta (YRD) region of China were simulated. By incorporating I/SVOC emissions into the model, the modeled average SOA concentrations in the region increased by 148%. Significant model improvements in the simulations of different OA components were demonstrated by comparing with the comprehensive observation data. Furthermore, spatial and seasonal variations of different source contributions to OA production were identified.

* Correspondence to C. Huang (huangc@saes.sh.cn)

26 We found cooking emissions are predominant sources of POA in the densely populated

27 urban area of the region. I/SVOC emissions from industrial sources are dominant

28 contributors to the SOA formation, followed by those from mobile sources. Our results

29 indicate that future control measures should be specifically tailored on intraregional

30 scale based on the different source characteristics to achieve the national goal of

31 continuous improvement in air quality. In addition, local source profiles and emission

32 factors of I/SVOCs as well as SOA formation mechanisms in model framework are

33 urgently needed to be updated to further improve the model performance and thus the

34 accuracy of source identifications.

35 **Key words:** semi-volatile and intermediate volatility organic compounds; secondary

36 organic aerosol; emission inventory; source contribution; model simulation

37 **1. Introduction**

38 Organic aerosol (OA) contributes a large fraction (20 to 90%) of atmospheric

39 submicron aerosol (Zhang et al., 2007; Jimenez et al., 2009) and has negative impacts

40 on air quality, climate (Shrivastava et al., 2017), and human health (Nault et al., 2021).

41 OA is composed of primary organic aerosol (POA) directly emitted from fossil fuel

42 combustion, biomass burning, and other sources, as well as secondary organic aerosol

43 (SOA) formed through the atmospheric oxidation of gas-phase species emitted from a

44 wide range of biogenic and anthropogenic sources (Hallquist et al., 2009).

45 Understanding and identifying the origins of OA is therefore important for elucidating

46 their health and climate effects and establishing effective mitigation policies. However,

47 OA is a dynamic system driven by the gas-particle partitioning of organic vapors and

48 particulate organic material and continuously evolves upon atmospheric oxidation

49 (Robinson et al., 2007; Donahue et al., 2009; Zhao et al., 2013; Jathar et al., 2014). It is

50 challenging to constrain the abundance of OA precursors and to identify key sources.

51 Great efforts have been made in the identification of OA sources through source

52 apportionment of the measured OA components, such as positive matrix factorization

53 (PMF) (Zhang et al., 2011), chemical mass balance (CMB) model (Zheng et al., 2002)

54   or multiline engine (ME-2) (Canonaco et al., 2013). The Aerodyne high-resolution

55   time-of-flight aerosol mass spectrometer (AMS), has been proven to be a powerful tool

56   in quantification and chemical characterization of different OA components in real-time

57   (Canagaratna et al., 2007). Coupled with PMF analysis, AMS measurements allow for

58   the deconvolution of physically meaningful OA factors. Commonly retrieved factors

59   include three POA sources, i.e. hydrocarbon-like OA (HOA) related to fossil fuel

60   combustion, biomass burning OA (BBOA), and cooking-related OA (COA), as well as

61   two SOA components, i.e. less oxidized oxygenated OA (LO-OOA) and more oxidized

62   oxygenated OA (MO-OOA) (Hayes et al., 2013; Crippa et al., 2014; Sun et al., 2014;

63   Li et al., 2017). Combining offline AMS and radiocarbon (^{14}C) measurements, Huang

64   et al. (2014) also identified the contributions of fossil and non-fossil sources to SOA.

65   Attempts have been made in subsequent studies by coupling the AMS measurement

66   with a suite of comprehensive and collocated SOA tracer measurements to distinguish

67   biogenic and major anthropogenic SOA sources, such as traffic and cooking emissions

68   (Xu et al., 2015; Zhang et al., 2018; Zhu et al., 2020; Huang et al., 2021a). However,

69   given the hard ionization in the AMS, there are limits to how much source information

70   can be extracted from AMS data. Further deconvolution on the contributions of

71   different sources to OA production is challenging.

72   Besides field measurements, air quality modeling is another widespread technique,

73   which has advantages for regional-scale OA source apportionment with higher temporal

74   and spatial resolution. However, the model simulated SOA concentration still has large

75   gaps with that measured in the atmosphere. The volatility basis set (VBS) scheme is

76   therefore developed, which lumps organic precursors as well as their oxidation products

77   into different volatility bins. Upon atmospheric aging, the volatility of these compounds

78   evolves due to the processes such as functionalization and fragmentation, which can be

79   accounted for in the models by shifting the volatility bins of these compounds (Donahue

80   et al., 2006). Previous studies have successively configured the VBS scheme from one-

81   dimensional (1-D) to 1.5-/2-dimensions (1.5-/2-D), which can better describe the

82   evolution of OA in the 2-D space of oxidation and volatility in the model, and coupled

83   the simplified emission inventory of SOA precursors estimated from POA to improve

84   the model performance on SOA simulation (Tsimpidi et al., 2010; Koo et al., 2014;

85   woody et al., 2016; Zhao et al., 2016a; Yang et al., 2019). However, there are still some

86   shortcomings in the modeling of OA, for example the lack of representation of the

87   hydrophilic properties of OA, which assumes SOA condenses onto an organic phase,

88   whereas SOA may also condense on an aqueous phase (Kim et al., 2011). Another

89   important constraint is the underestimation of intermediate-volatility organic

90   compounds (IVOCs) and semi-volatile organic compounds (SVOCs) emissions in the

91   models, which potentially have substantial contributions to SOA budget owing to their

92   high SOA yields (Presto et al., 2009; Tkacik et al., 2012; Zhao et al., 2014; Liggio et

93   al., 2016). IVOCs refer to organic compounds with effective saturation concentrations

94   (C*) between 10^3 to 10^6 $\mu g \cdot m^{-3}$ at 298 K and 1 atm, while SVOCs refer to organic

95   compounds with C* between 10^{-1} to 10^3 $\mu g \cdot m^{-3}$ at 298 K and 1 atm (Robinson et al.,

96   2007).

97   I/SVOC emission inventories have been developed and applied into air quality

98   models over the past decade. Most of them were estimated by applying different scaling

99   factors based on their relationship with POA, volatile organic compounds (VOCs), or

100   some proxies like naphthalene (Pye and Seinfeld, 2010; Shrivastava et al., 2011; Jathar

101   et al., 2017; Wu et al., 2019, 2021; Li et al., 2020, 2022; Ling et al., 2022). Yet in

102   practice, a same scaling factor was applied to most of the sources in previous studies

103   due to the lack of measurements on I/SVOC emission factors. For example, except

104   biomass burning (0.75–1.5), Wu et al. (2019) utilized scaling factors of 8–30 for all of

105   the other emission source categories, which was estimated based on the measurements

106   of on-road mobile source. Li et al. (2020) assumed scaling factors of 1.5 for on-road

107   mobile source, and 0.34–1.5 for the other sources, such as industrial and residential

108   sources, which were much lower than the estimations in Wu et al. (2020). Huang et al.

109   (2021b) have tried emission factor method to quantify the I/SVOC emissions, yet the

results were 60% lower than the scaling factor method, far from reproducing the measured amount of SOA. Obviously, roughly estimating I/SVOC emissions using one or two emission profiles as surrogates for all emission sources will create large uncertainties.

Recent studies have successively determined the volatility distribution, chemical composition, and emission factors of I/SVOCs from mobile sources, including gasoline and diesel vehicles, non-road diesel machinery, marine vessel, and aircraft (Presto et al., 2011; Cross et al., 2013; Zhao et al., 2015, 2016b; Huang et al., 2018; Qi et al., 2019; Drozd et al., 2019). I/SVOC emission profiles have been reported for nonmobile-sources as well, including coal combustion, wood-burning, cooking, fuel evaporation, and industrial and residential volatile chemical products (Huffman et al., 2009; Gentner et al., 2012; May et al., 2013; Koss et al., 2018; McDonald et al., 2018; Cai et al., 2019; Drozd et al., 2021), making the quantification of I/SVOC emissions and their involvement in air quality models possible.

In China, SOA has been emerging as an important contributor to air pollution. Field observations reveal that OA contributes significantly (30%) to the $PM_{2.5}$ concentrations in most parts of China (Tao et al., 2017; Liu et al., 2018b), among which the SOA contributes up to 80% of OA during haze pollution (Huang et al., 2014; Ming et al., 2017; Li et al., 2021). SOA formation in China has already been examined in several modeling studies. They found that by considering the POA aging and I/SVOCs oxidation in the models, which is realized by the coupling of VBS scheme, the formation and evolution of SOA can be much better simulated compared to the results of the two-product SOA modeling framework (Zhao et al., 2016a; Wu et al., 2019; Li et al., 2020; Yao et al., 2020; Huang et al., 2021b). Chang et al. (2022) developed a full-volatility organic emission inventory with source-specific I/SVOC emission profiles for China, which have greatly improved the model performance on SOA concentrations. However, large gaps still exist between the observed and modeled SOA. Studies on high-resolution I/SVOC emission inventory for more specific sources are highly needed.

138   In this study, taking the Yangtze River Delta (YRD) region, including Jiangsu,

139   Zhejiang, Anhui provinces and Shanghai city, as a pilot, we established a high-

140   resolution source specific I/SVOC emission inventory. We then applied the established

141   inventory into CMAQ v5.3 to evaluate the contributions of I/SVOC emissions to SOA

142   formation by comparing the results with the observation data collected in the region.

143   Furthermore, we also run the model in different scenarios to quantify the seasonal

144   contributions of different sources to POA and SOA formation in the YRD region.

145   **2. Materials and methods**

146   2.1 I/SVOC emission inventory

147   Previous studies usually used POA scaling factors to estimate the I/SVOC

148   emissions, which may lead to large uncertainties in the estimation of gas-phase organic

149   compound-dominated sources, like oil refinery, chemical production, and industrial

150   solvent-use. Herein, we compiled both gas-phase and particle-phase I/SVOCs emission

151   inventories and incorporate them into the model. Detailed process of the inventories is

152   as follows.

153   (1) Source classification: To refine the I/SVOC emissions from different sources,

154   we divided the sources into five major categories and then further grouped them into

155   21 sub-categories. The major categories include industrial process sources, industrial

156   solvent-use sources, mobile sources, residential sources, and agricultural sources. As

157   shown in Table S1, the industrial process sources include the sectors such as oil refinery,

158   chemical production, and pulp and paper production; Industrial solvent-use sources

159   include textile, leather tanning, timber processing, and various industrial volatile

160   chemical products use; Mobile sources include gasoline and diesel vehicle emissions,

161   fuel evaporation, diesel machinery, marine vessel, and aircraft; Residential sources

162   include coal combustion, residential solvent-use, and cooking emissions; Agricultural

163   source is specifically referred to biomass burning in household stoves, and open burning

164   was not included in this study.

165   (2) Emission estimation: Gas-phase emissions for each specific source were

166   estimated by the ratios of total I/SVOC components to anthropogenic VOC (AVOC)

167   components (G-ratio). Similarly, particle-phase emissions were estimated by the ratios

168   of total particle-phase I/SVOC components to POA (P-ratio). The G- and P-ratios for

169   each source were determined according to their fractions of total I/SVOC species in

170   VOC and POA emissions. Then we grouped different I/SVOC species into lumped

171   I/SVOC bins based on their C^* to determine the volatility distributions of each source.

172   The gas-phase emissions were distributed into four lumped aliphatic IVOC bins across

173   the volatility basis set from $C^*=10^3$ to 10^6 $\mu g \cdot m^{-3}$, two aromatic IVOC bins with the

174    $C^*=10^5$ and 10^6 $\mu g \cdot m^{-3}$, and four lumped SVOC bins with C^* from 10^{-1} and 10^2 $\mu g \cdot m^{-3}$

175    $^{-3}$. The particle-phase emissions were distributed into five bins spanning C^* from 10^{-1}

176   and 10^3 $\mu g \cdot m^{-3}$. Source profiles of I/SVOC species for different sources were referenced

177   from the results in previous studies. Table S1 and S2 show the G-ratios and P-ratios for

178   each specific source and their references. For industrial process, industrial solvent-use,

179   and residential solvent-use sources, only gas-phase emissions were considered. Their

180   G-ratios and emission profiles were derived from the latest version of SPECIATE 5.1

181   database (US EPA, 2021). For gasoline and diesel vehicles, the G-ratios and P-ratios

182   and emission profiles were referenced from a new mobile-source parameterization

183   recommended by Lu et al. (2020). Those of diesel machinery, marine vessel, and

184   residential coal combustion were determined by recent measurement results in China

185   (Qi et al., 2019; Huang et al., 2018; Cai et al., 2019). The G-ratios and profiles of

186   cooking and biomass burning emissions were derived from SPECIATE 5.1 database,

187   while their P-ratios and profiles were referenced from two previous studies (May et al.,

188   2013; Louvaris et al., 2017). The base emissions of AVOCs and POA (See Table S3)

189   were taken from a high-resolution emission inventory for the year of 2017 developed

190   in our previous study (An et al., 2021).

191   (3) Model input: Before being input into the model, the estimated gas-phase and

192   article-phase emissions were summed and then redistributed according to their phase

193   equilibrium under the actual atmospheric state. The formula of phase equilibrium is

194 shown in Equation (1).

$$F_\text{p} = \frac{c_\text{OA}}{c_\text{OA}+c^*} \tag{1}$$

196 Where, F_p is the fraction of particle-phase emissions for each volatility bin. C_OA

197 represents the OA concentration in the atmosphere. We assumed it to be 10 μg·m⁻³ in

198 this study. C^* is the effective saturation concentration of each volatility bin. After

199 redistribution, the I/SVOC emissions for each source category were allocated into 4 km

200 × 4 km grids and hourly temporal profiles using the same method as the criteria

201 pollutants.

202 2.2 Model configuration

203 　　We used Community Modeling and Analysis System (CMAQ version 5.3.2) to

204 simulate the concentrations of air pollutants. The domain of the simulation is presented

205 in Figure 1. The simulations were conducted for three nested grids with horizontal

206 resolution of 36 km (D1), 12 km (D2) and 4 km (D3), respectively. D1 covers most of

207 China and the surrounding countries including Japan and South Korea; D2 covers

208 eastern China and D3 covers the entire YRD region and its surrounding land and waters.

209 　　Meteorological fields were provided by the Weather Research and Forecasting

210 (WRF version 3.7) model with 27 vertical layers extending to the tropopause (100 hpa).

211 The initial and boundary conditions (ICs, BCs) in the WRF were based on the 1° × 1°

212 reanalysis data from the National Centers for Environmental Prediction Final Analysis

213 (NCEP-FNL). Physical options used in the WRF simulation are listed in Table S4.

214 　　The　　Sparse　　Matrix　　Operator　　Kernel　　Emissions　　(SMOKE,

215 https://cmascenter.org/smoke) model was applied to process emissions for input to

216 CMAQ. CMAQ version 5.3.2 (https://cmascenter.org/cmaq/) was used to simulate

217 atmospheric pollutants concentrations. ICs and BCs of D1 domain are based on a Model

218 For Ozone And Related Chemical Tracers (MOZART) global simulation

219 (https://acom.ucar.edu/wrf-chem/mozart.shtml). For the inner D2 and D3 domain, ICs

220 and BCs are extracted from the simulation results of the outer domains. Options selected

221 for the CMAQ simulations include the SAPRC07 gas phase chemistry, the AERO7

aerosol scheme, the Regional Acid Deposition Model (RADM) model aqueous phase chemistry, and ISORROPIA inorganic particulate thermodynamics.

The emission inventory developed in this study was used to produce the emission system in the YRD region while emissions beyond YRD were supplied by Multiresolution Emission Inventory for China (MEIC-2017, http://meicmodel.org), Shipping Emission Inventory Model (SEIM) (Liu et al., 2016), and the Model Inter-Comparison Study (MIX) emission inventory for 2010 (Li et al., 2017). The I/SVOC emission inventory outside the YRD region was developed by multiplying the VOCs and POA emissions with the average G-ratios and P-ratios of major source categories like industry, vehicle, marine vessel, and residential. Biogenic volatile organic compounds (BVOCs) emissions were estimated based on MEGAN (the Model of Emissions of Gases and Aerosols from Nature) version 2.10 driving by inputs of the leaf area index (LAI) from MODIS product, plant functional types (PFT) base on remote sensing data, inline coupled emission factors and meteorology simulated by the WRF model. Detail configurations of MEGAN can be obtained from our previous study (Liu et al., 2018a).
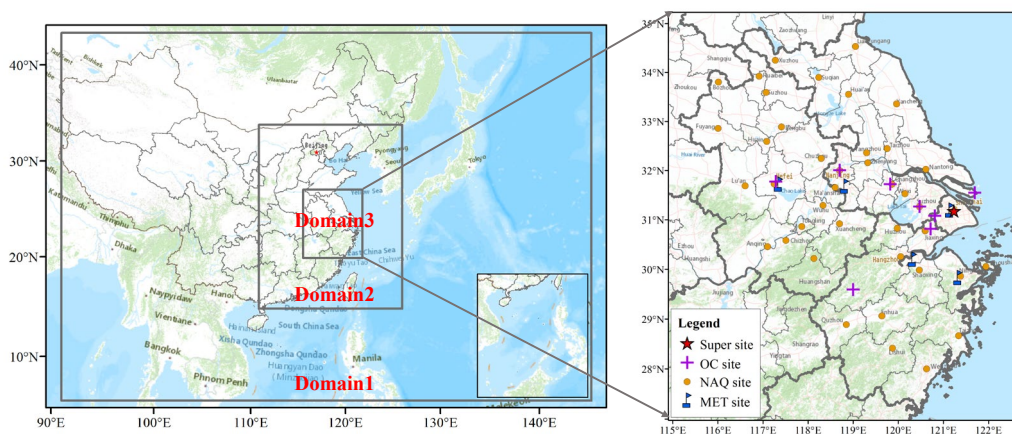
Figure 1. Modeling domain and locations of observation sites. The blue marks are meteorological monitoring sites. The yellow dots represent the national air quality monitoring sites. The purple crosses are the observation sites with $PM_{2.5}$ chemical composition measurements. The red star represents the observation site of AMS measurement.

SOA formed from I/SVOCs was estimated using the parameterization within the

244   VBS framework in Lu et al. (2020). Specifically, the I/SVOC surrogates react with OH,

245   generating four oxygenated organic species with volatility spanning from $C^* = 10^{-1}$ to

246   10^2 $\mu g \cdot m^{-3}$, which may exist in both gas and condensed phase. The rate coefficient (i.e.,

247   k_{OH}) and product yields (i.e., α_i, i=1, 2, 3, 4) for each primary I/SVOC species were

248   derived based on previous laboratory results (Zhao et al., 2015; Zhao et al., 2016b).

249   Multi-generation oxidation was considered by implementing further oxidation of the

250   vapors from the initial oxidation, which redistributes the mass across the volatility bins

251   of $C^* = 10^{-2}$ to 10^2 $\mu g \cdot m^{-3}$, and thus fragmentation and functionalization were included.

252   It is worth noting that only one-step oxidation of the vapor products was considered,

253   using the default aging scheme for the oxidation products of POA in the CMAQ

254   (Murphy et al., 2017). Additionally, SOA formation from SVOCs were treated similarly,

255   and more details can be found in Murphy et al. (2017). POA was treated as semivolatile

256   to account for its gas-particle partitioning and ageing process and segregated to several

257   particle species, which varied in their volatility that quantified with the metric $C^* = 10^{-1}$

258   ^{1} to 10^3 $\mu g \cdot m^{-3}$ (Donahue et al., 2006). Particle-phase emissions from different sources

259   were then speciated and input as semivolatile accordingly. The remaining POA

260   emissions excluding particle-phase I/SVOCs were treated as nonvolatile POC (primary

261   organic carbon) and PNCOM (primary non-carbon organic matter).

262   2.3 Model simulations

263   To investigate the model performance on OA simulations and the contributions of

264   different sources, we set 14 simulation cases using brute-force method (Zhang et al.,

265   2005). Table 1 shows the settings for these 14 cases. First was BASE simulation case,

266   in which the I/SVOC emissions was not included and the POA emissions were treated

267   as non-volatile. The second was the I/SVOC-E case, which augmented the high-

268   resolution I/SVOC emission inventory established in this study. In addition, the POA

269   emissions in the I/SVOC-E simulation were split into both non-volatile and semivolatile

270   parts. The non-volatile emissions were obtained by subtracting the P-ratios from the

271   total POA. The semivolatile emissions, that was particle-phase, were treated with

272 variable gas–particle partitioning and multigenerational aging in this simulation case.

273 We then used the difference between I/SVOC-E and BASE cases to evaluate the OA

274 contributions from I/SVOC emissions. CASE1 to CASE12 respectively excluded the

275 VOC and I/SVOC emissions from different sources. We used the differences between

276 I/SVOC-E and CASE1−12 to quantify the contribution of each source to OA

277 concentration.

278 **Table 1.** Settings of simulation cases.

Name	Sources with added I/SVOC emissions
BASE	none
I/SVOC-E	all
CASE1	all except industrial process
CASE2	all except industrial solvent-use
CASE3	all except mobile sources
CASE4	all except residential sources
CASE5	all except biomass burning
CASE6	all except biogenic sources
CASE7	without VOCs and I/SVOC emissions
CASE8	all except gasoline vehicle
CASE9	all except diesel vehicle
CASE10	all except diesel machinery
CASE11	all except marine vessel
CASE12	all except cooking

279 2.4 Model evaluation

280   To capture the characteristics of OA with different meteorological features in the

281 YRD region, we selected four periods to represent spring (Mar. 15th to Apr. 15th, 2019),

282 summer (Jul. 1st to 31st, 2019), autumn (Oct. 15th to Nov. 15th, 2018), and winter (Dec.

283 1st to 31st, 2018) to conduct the simulations. Evaluations on model performance were

284 made by comparing the simulation results with the observations obtained in the region,

285 including 5 meteorological observation sites, 10 $PM_{2.5}$ chemical composition sites, and

286 41 national air quality monitoring sites, one in each city. The locations of the

287 meteorological and air pollutant observation sites are shown in Figure 1.

288   We also used the observation data of an AMS and a GC-MS/FID system at the

289 supersite in Shanghai to further verify the model performance on the simulation of POA,

SOA, and key VOC precursors. Details of AMS measurements and PMF analysis are provided in our previous study (Huang et al., 2021a). A total of 55 PAMS (Photochemical Assessment Monitoring Stations) species were identified by the GC-MS/FID system including 27 alkanes, 11 alkenes, acetylene and 16 aromatics. The supersite was located on the top-floor of an eight-story building in Shanghai Academy of Environmental Sciences (SAES, 31°10' N, 121°25'E), 30 m above the ground. The site was in a typical residential and commercial area with significant influence from traffic emission. Several petrochemical and chemical industrial factories sit around 50 km away from the site to the south and southwest.

Model performance in simulation of meteorological parameters and major criteria air pollutants are summarized in Table S5 and S6. The mean bias (MB), mean gross error (MGE), root-mean-square error (RMSE), and index of agreement (IOA) of temperature, humidity, wind speed, and wind direction in each season are within the criteria recommended by Emery et al. (2001). Although the temperature in summer and winter, and wind speed in autumn and winter were slightly overestimated, their MGE and IOA values are within the uncertainties as recommended in Emery et al. (2001).

For the simulation of major criteria air pollutants, both mean fractional bias (MFB) and mean fractional error (MFE) of all pollutants met the criteria recommended by Boylan and Russell (2006). Since the addition of I/SVOC emissions would change the $PM_{2.5}$ simulation results, we thus presented the statistical results for both BASE and I/SVOC-E cases in the Table S6. The simulated SO_2 was slightly overestimated, which might be caused by the overestimation of SO_2 emissions due to the fact that China's SO_2 emission reduction was far beyond the expectation. In contrast, the modeled NO_2 were underestimated in spring, autumn, and winter, likely due to the overestimation of wind speed in these seasons. The modeled O_3 and $PM_{2.5}$ were slightly overestimated in the I/SVOC-E simulation case. Overall, the simulated meteorological parameters and major criteria air pollutants are consistent with the observations.

317   **3. Results and discussion**

318   3.1 I/SVOC emission inventory

319   3.1.1 Source-specific I/SVOC emissions

320   Table 2 shows the gas-phase and particle-phase emission inventories for detailed

321   source category for year 2017 in the YRD region. The total gas-phase emission in the

322   YRD region was 1148 Gg in 2017, lower than that in Wu et al. (2021) of 1360 Gg, but

323   higher than the estimate in Huang et al. (2021b) of 730 Gg. We found industrial solvent-

324   use was the largest contributor (484 Gg, 42.1%) of total gas-phase emissions, followed

325   by industrial process sources (245 Gg, 21.3%), mobile source (344 Gg, 30.0%),

326   residential source (62 Gg, 5.4%), and agriculture source (14 Gg, 1.2%). Specifically,

327   chemical production, textile, and solvent-based coating were major sectors of gas-phase

328   emissions in the YRD region, accounting for 20.8%, 19.5%, and 15.1% of the total gas-

329   phase emission, and their contributions to AVOC emissions were 20.7%, 2.2%, and

330   23.4%, respectively (See Table S3). The chemical materials and production process of

331   these industries were quite different, which would make their G-ratios quite different in

332   the profiles. For example, the textile industry only accounted for 2.2% of the total

333   AVOC emissions in the YRD region but contributed to 19.5% of the gas-phase

334   emissions due to its higher G-ratio (2.473). Another example is water-based coatings,

335   whose VOC emissions were approximately 10.2% of solvent-based coatings, while

336   their I/SVOC emissions were 29.1% of those from solvent-based coatings. These

337   findings indicate that reductions in VOC emissions not necessarily corresponds to the

338   simultaneous reductions in I/SVOCs emissions and subsequent SOA formation, which

339   should be considered in future control strategies (Yuan et al., 2010).

340   For gas-phase emission of mobile origin, the major contributors were gasoline

341   vehicle, diesel vehicle, and non-road diesel machinery, accounting for 13.6%, 11.7%,

342   and 2.1%, respectively. The total gas-phase emissions from gasoline and diesel vehicles

343   were 291 Gg, much higher than the results reported in Liu et al. (2017) (30 Gg) and

344   Huang et al. (2021b) (16 Gg) using the emission factor method, which likely

underestimates the emission factors of I/SVOCs due to the lack of localized emission factors. Our tunnel experiment results show that the average IVOCs emission factors of gasoline and diesel vehicles were 15.3 mg·km^{-1} and 219.8 mg·km^{-1} (Tang et al., 2021), which were significantly higher than those used in the above studies (Liu et al., 2017; Huang et al., 2021b). More comprehensive localized emission measurements are advocated to better constrain the I/SVOC emissions from mobile sources.

Particle-phase emissions were 83 Gg. The largest contributor of particle-phase emissions came from cooking emission and diesel vehicle, accounting for 53.2% and 119% of the total, followed by gasoline vehicle (5.2%), marine vessel (2.7%), diesel machinery (2.5%), and biomass burning (1.8%). Note that the particle-phase emissions from coal combustion (e.g. power plants, boilers, etc.), other industrial processes, and aircraft were not included in this study. On the one hand, the POA emissions (See Table S3) from these sources were limited, accounting for less than 5%, which could be expected that their particle-phase emissions were also relatively low. On the other hand, the profiles of particle-phase components of these sources were still difficult to obtain. More measurements of the I/SVOC emissions from these sources is very necessary in the future.

Table 2. Source-specific emissions of I/SVOCs for the year 2017 in the YRD region.

Source		I/SVOCs		Gas-phase		Particle-phase	
		Gg	%	Gg	%	Gg	%
Industrial process	Oil refinery	5.63	0.46	5.62	0.49	0.01	0.01
	Chemical production	244	19.8	239	20.8	4.69	5.65
	Pulp and paper	0.11	0.01	0.11	0.01	0.00	0.00
Industrial solvent-use	Textile	230	18.7	224	19.5	5.72	6.90
	Leather tanning	3.83	0.31	3.83	0.33	0.00	0.00
	Timber processing	31.1	2.52	31.1	2.71	0.00	0.00
	Furniture coating	1.32	0.11	1.32	0.12	0.00	0.00
	Solvent-based coating	173	14.1	173	15.1	0.00	0.00
	Water-based coating	50.3	4.09	50.3	4.38	0.01	0.01
	Dry cleaning	0.02	0.00	0.02	0.00	0.00	0.00
	Paint remover	0.01	0.00	0.01	0.00	0.00	0.00
Mobile source	Gasoline vehicle	161	13.1	157	13.6	4.34	5.23

	Diesel vehicle	144	11.7	134	11.7	9.86	11.88
	Fuel evaporation	0.69	0.06	0.69	0.06	0.00	0.00
	Diesel machinery	49.6	4.03	47.51	4.14	2.11	2.54
	Marine vessel	7.12	0.58	4.91	0.43	2.21	2.66
	Aircraft	0.64	0.05	0.64	0.06	0.00	0.00
	Coal combustion	2.73	0.22	2.73	0.24	0.00	0.00
Residential source	Residential solvent-use	35.3	2.87	35.2	3.07	0.09	0.11
	Cooking	76.8	6.23	24.3	2.12	52.5	63.2
Agriculture source	Biomass burning	15.0	1.22	13.6	1.18	1.45	1.75
	Total	1231	100	1148	100	83.0	100.00

363   3.1.2 Volatility distributions of I/SVOCs

364   Figure 2 shows the volatility distribution of I/SVOC emissions from different

365   sources as well as their gas-particle distributions. The I/SVOC emissions generally

366   showed an increasing trend with the increase of volatility. As shown in Figure 2(a),

367   IVOC emissions (logC* bins at 3−6) accounted for 86% of the total I/SVOC emissions,

368   overwhelmingly dominated by industrial process and mobile sources. SVOCs (logC*

369   bins at 0−2) and low-volatile organic compounds (LVOCs, logC* bins at -1) contributed

370   to 11% and 3% of the total I/SVOCs emissions. In terms of the contributing sectors,

371   mobile sources, industrial process, and solvent-use dominated the total I/SVOC

372   emissions. While the IVOCs were equally contributed by above-listed three sources,

373   residential and mobile sources dominated the SVOCs and LVOCs emissions.

374   We further investigated the contributions of different volatility bins to each source

375   category. The mobile source was dominated by IVOC emission (88%). Note that IVOC

376   emissions from vehicles included a certain fraction of aromatics, which have faster OH

377   reaction rates and higher SOA yields compared to aliphatics in the same volatility bin

378   (Zhao et al., 2016b; Drozd et al., 2019). Lu et al. (2020) therefore defined two additional

379   lumped IVOC species with logC* bins at 5 and 6 to account for the aromatic IVOCs in

380   vehicle exhaust according to the measurements in previous studies (Zhao et al., 2015;

381   Zhao et al., 2016b). Here in this study, we also split the aromatic IVOC emissions from

382   mobile sources and found that aromatic IVOCs accounted for 23% of the total I/SVOC

383   emissions from the mobile source. The industrial process and solvent-use sources were

also dominated by IVOC emissions, accounting for 81% and 97%, respectively. The volatility distribution of residential sources was relatively uniform, with IVOCs, SVOCs and LVOCs accounting for 40%, 30%, and 30%. Agricultural (i.e., biomass burning) sources were more concentrated in IVOCs, accounting for 76%, while SVOCs accounted for 24%. It should be noted that other than mobile sources, the emission profiles of the other sources were mainly derived from SPECIATE 5.1 database (US EPA, 2021) in this study, which may be inconsistent with real-world emissions in China. To further reduce the uncertainty in the I/SVOC emission inventory, measurements of I/SVOC emissions from different local sources are therefore important and urgently needed in the future.
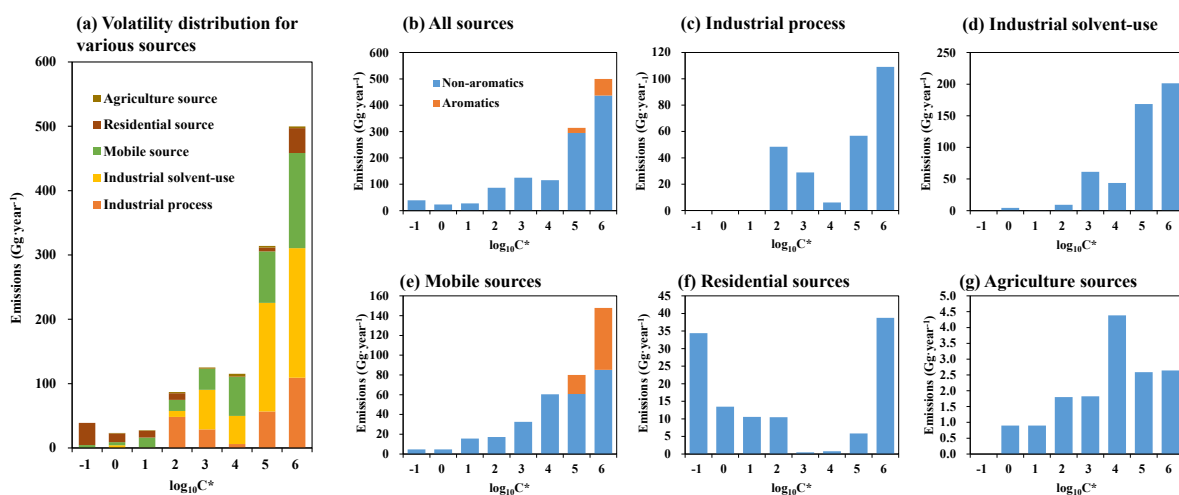
**Figure 2.** Volatility distributions of I/SVOCs emitted from different sources in the YRD region.

3.1.3 Spatial distributions of I/SVOC emissions in YRD region

Figure 3 compares the spatial distributions of AVOC, IVOC, SVOC, and LVOC emissions in the YRD region. The IVOC, SVOC, and LVOC emissions were largely concentrated in city clusters in eastern YRD, and hotspots can also be observed in the northern agglomerations. The distributions of I/S/LVOC emissions were generally consistent with that of the AVOC emissions in the region. Compared to the spatial distributions of I/S/LVOC emissions in Chang et al. (2022), our emissions had similar spatial distributions but at a higher resolution. Emission hotspots in urban areas can be captured more clearly in this study, which will help improve the simulation in urban

405   areas.

406   Figure 4 shows the spatial distributions of source-specific I/SVOC emissions in

407   the YRD region. There were considerable differences in the spatial distributions of

408   I/SVOC emissions from different sources. The I/SVOC emissions from industrial

409   sources (including industrial process and industrial solvent-use) were mainly

410   concentrated in the eastern urban agglomeration, which was related to the developed

411   industrial activities in the region. The I/SVOC emissions from mobile and residential

412   sources clustered into multiple hotspots in urban areas, while emissions from

413   agricultural sources were mainly distributed in northern YRD, where frequent

414   agricultural activities exist.

415   We also compare the spatial distributions of I/SVOC emissions with those of POA

416   and BVOCs. We found that POA emissions were more concentrated in urban centers

417   associated with mobile and residential sources (See Figure S1). BVOC emissions in the

418   YRD region were mainly distributed in the southern area, where AVOC and IVOC

419   emissions were relatively low. The difference in the spatial distributions of I/SVOC,

420   AVOC, BVOC, and POA emissions implies that the sources of organic components in

421   different areas of the region are quite different, which will be discussed in the following
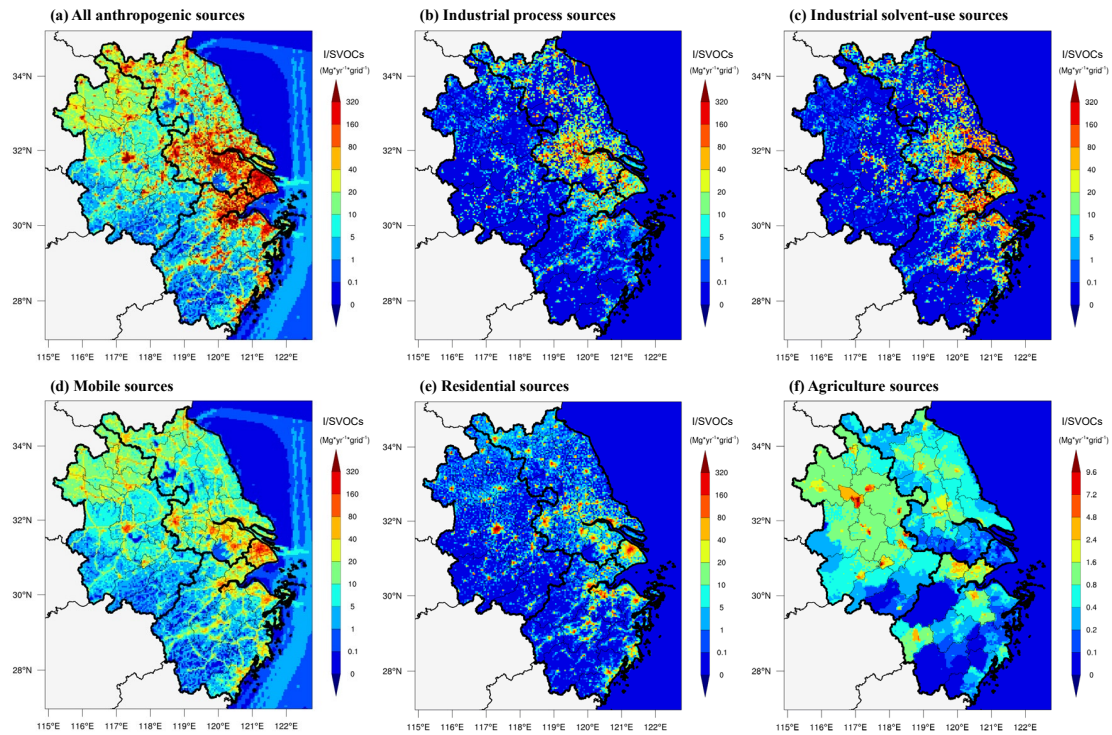
422   sections.
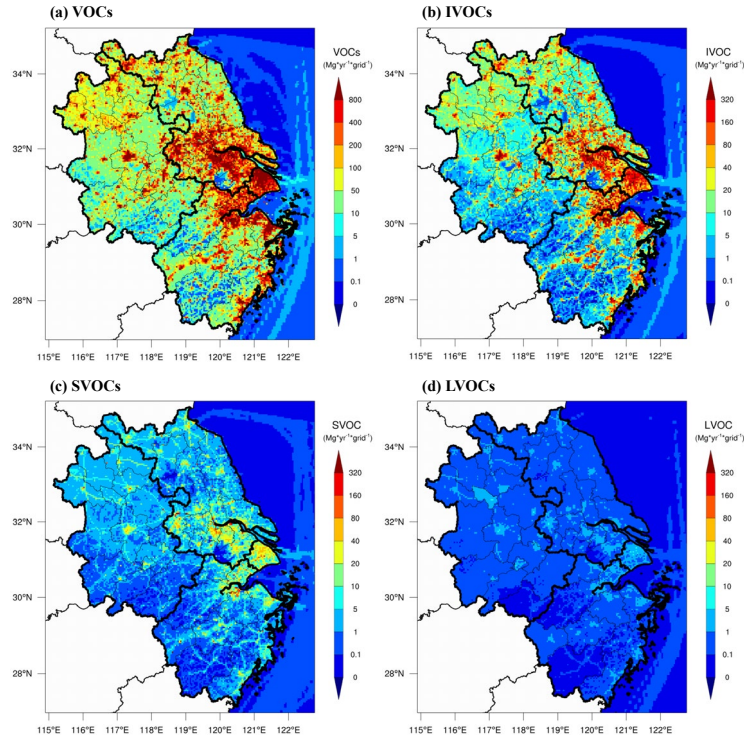
Figure 3. Spatial distributions of anthropogenic VOC, IVOC, SVOC, and LVOC emissions in the YRD region for the year 2017.

Figure 4. Spatial distributions of I/SVOC emissions from different source categories in the YRD region for the year 2017.

429 3.2 Comparison between model simulation and observation

430 3.2.1 Simulation results of VOCs and IVOCs

431   Since model performance on the simulation of VOCs are critical for SOA

432 estimation, we first compare the modeled concentrations of VOCs with those of the

433 measured at the SAES supersite for several aromatic VOCs, including benzene, toluene,

434 and m-/p-/o-xylenes. As shown in Figure S2, the model simulation was able to capture

435 the hourly variations of these species measured, with Pearson correlation coefficients

436 (r) of 0.54−0.65, 0.45−0.60, 0.54−0.69 for toluene, xylene, and benzene respectively.

437 Although the simulation results of toluene were 28% lower and xylene and benzene

438 were 41% and 22% higher than those of the measured, the model results are within the

439 uncertainties. Overall, the simulation results of the VOC species showed good

440 agreements with the observations, which could be further used for the model simulation

441 of SOA formation.

442   Long-term continuous observations of I/SVOC concentrations were sparse, so the

443 simulation results of IVOCs were compared with those obtained from offline

444 measurements reported in our previous studies (Li et al., 2019; Ren et al., 2020). The

445 reported IVOC concentrations (sum of gas- and particle-phase concentrations) in

446 summer and winter Shanghai in 2018 respectively varied between 1.5−17.2 and

447 2.2−43.1 $\mu g \cdot m^{-3}$ with average concentrations of 6.8 ± 3.7 and 18.2 ± 11.0 $\mu g \cdot m^{-3}$. In

448 this study, our modeled average concentrations of IVOCs in spring, summer, autumn,

449 and winter at the SAES supersite in Shanghai were 12.8 ± 5.6, 9.0 ± 3.2, 12.2 ± 5.2,

450 and 12.4 ± 7.6 $\mu g \cdot m^{-3}$, respectively. The modeled IVOCs was higher in summer while

451 lower in winter, not to mention the diurnal patterns and spatial distributions also

452 remained unknown. This may be due to the difference in monthly profiles of I/SVOC

453 emissions, which has not been considered in this study. Another important reason

454 should be the chemical mechanism of IVOCs to SOA evolution still needs to be

455 improved. Continuous long-term measurements of I/SVOC at multiple locations are

456 strongly recommended in the future to help to improve the SOA model performance.

457   3.2.1 Simulation results of OA concentrations

458   Figure 5 presents the OA concentrations originated from different sources,

459   including POA and SOA formed from AVOCs, BVOCs, and I/SVOCs, in four seasons

460   in YRD from both BASE and I/SVOC-E simulations. Here we used the average of the

461   modeled concentrations at 41 national air quality monitoring sites (See the yellow dots

462   in Figure 1) to represent the regional average. The regional average concentration of

463   OA (8.8 μg·m^{-3}) in the I/SVOC-E simulation was 22% higher than that from BASE

464   simulation (7.2 μg·m^{-3}) due to the involvement of I/SVOCs in the I/SVOC-E simulation.

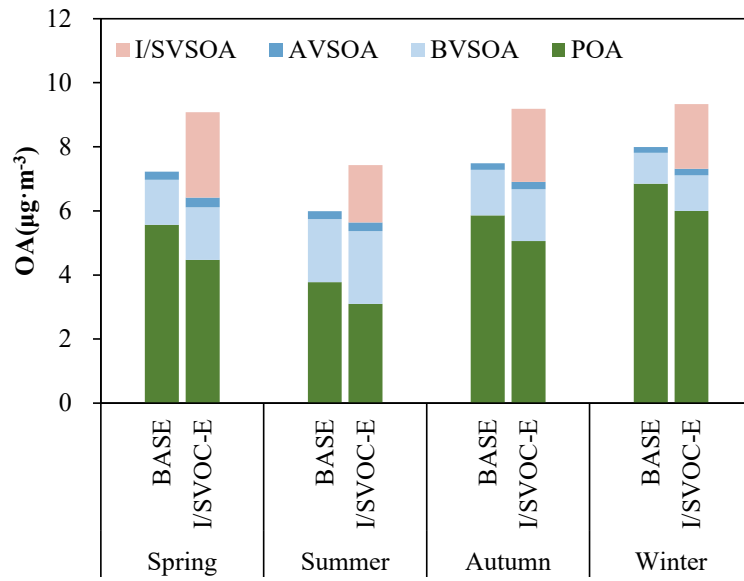465   The seasonal average concentration of POA was 5.5 μg·m^{-3} in the BASE case, with

466   the lowest in summer (3.8 μg·m^{-3}) and the highest in winter (6.9 μg·m^{-3}). High POA

467   concentrations in winter was mainly induced by the stagnant meteorological conditions

468   such as low wind speed and boundary layer height and weaker photochemical effect,

469   and vice versa in summer. For the spatial distributions as presented in Figure 6, POA

470   concentrations in northern YRD were high and mainly concentrated in urban areas,

471   which was consistent with the distributions of POA emissions (Figure S1). The POA

472   concentrations in the I/SVOC-E simulation decreased by 12%−20% compared with the

473   BASE case. In the I/SVOC-E simulation, the POA was treated as semi-volatile, where

474   gas–particle partitioning and multigeneration oxidation were considered (Murphy et al.,

475   2017). Entering into the atmosphere, more semi-volatile compounds evaporated into

476   gas-phase and then generated SOA through multigeneration oxidation, which reduced

477   the POA concentrations relatively.

478   The seasonal average concentration of AVSOA in the BASE case was only 0.2

479   μg·m^{-3}. The average AVSOA concentration in the I/SVOC-E case increased by 17%

480   compared with the BASE case due to higher OA loading. Nonetheless, AVSOA still

481   exhibited very limited contribution to the regional OA concentration, whereas average

482   concentration of BVOC derived SOA (BVSOA, 1.7 μg·m^{-3} in the I/SVOC-E simulation

483   case) was much higher. Also, evident seasonal variations were observed for BVSOA,

484   with the highest in summer (2.3 μg·m^{-3}), followed by spring (1.7 μg·m^{-3}), autumn (1.6

485 μg·m⁻³), and winter (1.1 μg·m⁻³). Hotspots of BVSOA concentrations were concentrated

486 in the western and southern YRD. The observed seasonal variations and spatial

487 distributions of BVOC derived SOA were consistent with those of the BVOC emissions

488 in YRD (Liu et al., 2018a).

489   The average concentration of I/SVOC derived SOA (I/SVSOA) in I/SVOC-E

490 simulation was 2.2 μg·m⁻³, with the highest in spring (2.7 μg·m⁻³) and the lowest in

491 summer (1.8 μg·m⁻³), which was a combined effect of emission, oxidation and

492 meteorological conditions. For example, Qin et al. (2022) suggested that in spring the

493 enhanced solar radiation and OH oxidation potentially promote the secondary

494 conversion from I/SVOCs to SOA. The low concentration in summer was likely due to

495 the better meteorological conditions than the other seasons. By incorporating I/SVOC

496 emissions into the I/SVOC-E simulation, the modeled average SOA concentration in

497 the region increased from 1.7 (BASE) to 4.1 μg·m⁻³; and high concentrations of

498 I/SVSOA were observed in central and northern YRD. Overall, the addition of high-

499 resolution I/SVOC emissions significantly increase the SOA concentration by 148%,

500 which will be further constrained by the observation in next section.

501   To validate the model performance on regional OA simulation, we compared it

502 with the measured concentrations of organic carbon (OC) in PM$_{2.5}$ at multiple sites in

503 the YRD region (Figure S3). Although both BASE and I/SVOC-E simulations showed

504 good correlations with the observation as shown in Figures S3c, S3f, S3i, and S3l, OC

505 concentrations in I/SVOC-E simulations in different seasons were all higher than those

506 in the BASE simulations. In the BASE simulation, the modeled OC concentrations of

507 each season only explained 51% to 71% of the observations. With the addition of

508 I/SVOC emissions into I/SVOC-E simulation, the modeled OC concentrations much

509 better agreed with the observations, with modeled OC increased to 70% to 91% of the

510 observations. Details for the statistical evaluation of model performance on OC in

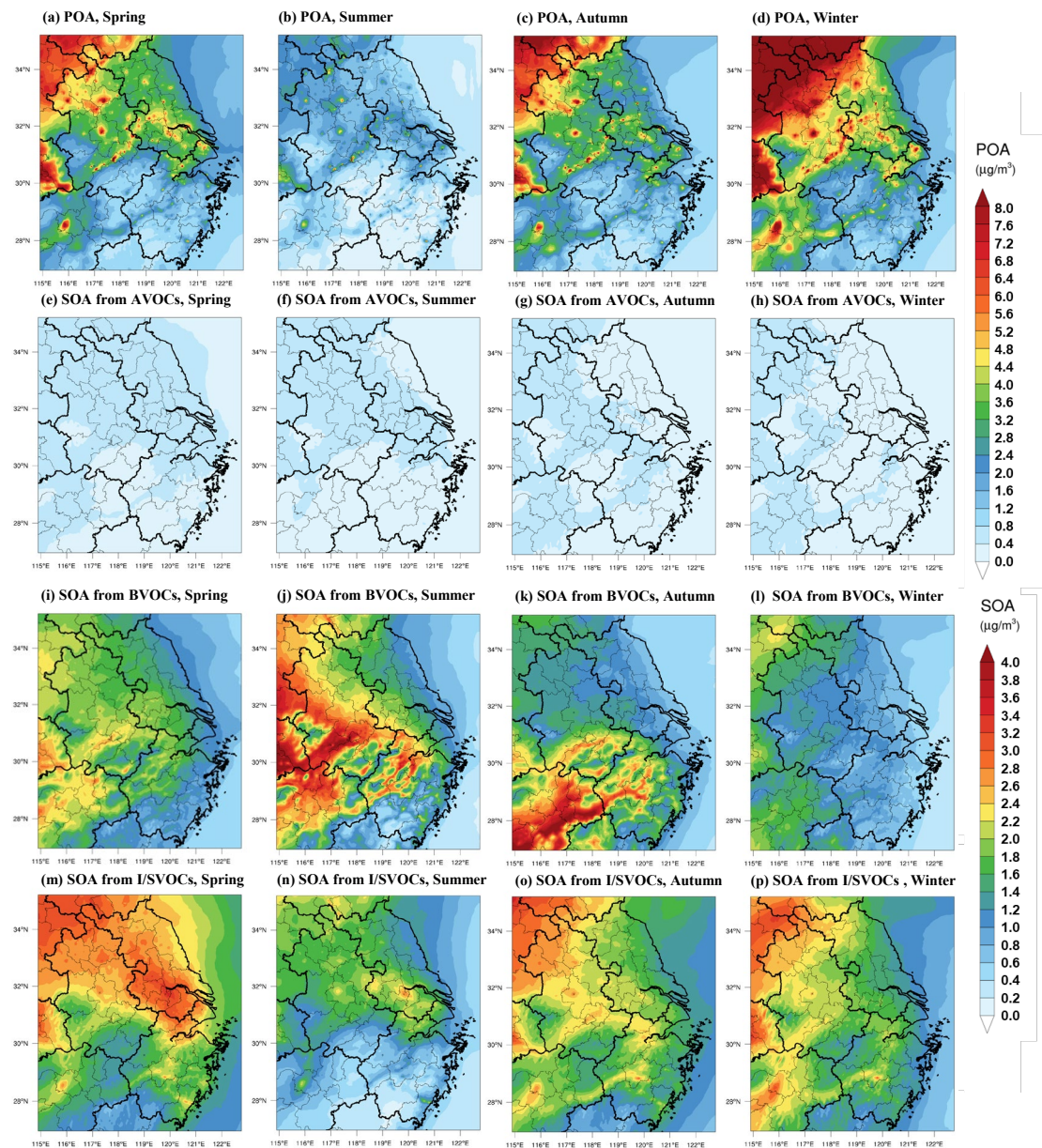511 BASE and I/SVOC-E simulations are shown in Table S7.

512

Figure 5. Comparisons of the regional average concentrations of POA and SOA formed from AVOCs, BVOCs, and I/SVOCs in different seasons from the BASE and I/SVOC-E simulations.

Figure 6. Spatial distributions of modeled POA and SOA formed from AVOCs, BVOCs, and I/SVOCs in different seasons in the I/SVOC-E simulation.

3.2.2 Temporal variations of OA components: simulation vs. AMS observation

To further validate the model performance on the simulations of POA and SOA, we compared the simulation results with those measured by an AMS at the SAES supersite. Both simulation and observation results were obtained for PM_1 aerosol particles (aerodynamic diameter < 1 μm). Note that uncertainty exist when directly compare the modeled OA factors with those resolved by AMS-PMF analysis since a clear split of POA and SOA from a measurement point of view can hardly be achieved.

525 To minimize the uncertainty associated with the PMF analysis, comprehensive

526 molecular identification of OA components was conducted and multiple source

527 apportionment model results were compared following the method in Huang et al.

528 (2021a) to improve the accuracy of the factor separation. Figure 7 shows that the

529 simulation results of POA, SOA and OA were similar to the observation results not only

530 in average concentration levels but also in temporal variations. For POA, the diurnal

531 patterns in the BASE and I/SVOC-E simulations agree with each other and both can

532 reproduce the observed concentrations. The POA concentrations in the I/SVOC-E

533 simulation cases decreased by 4%−18% (Figure S4) compared with the BASE case and

534 was closer to the observations. Similar to the observation results, the simulated POA

535 concentrations peaked at noon and early evening, which were mainly contributed by

536 cooking emissions as reported in our previous study (Huang et al., 2021a).

537 For SOA, the average concentrations in spring, summer, autumn, and winter in

538 BASE simulation were 1.2, 1.6, 0.8, and 0.7 $\mu g \cdot m^{-3}$, respectively, which were only

539 14%−30% of those observed by the AMS (see Figure S4). The SOA simulation was

540 improved in I/SVOC-E simulation with the modeled SOA concentrations of 3.8 3.7, 2.7,

541 and 2.3 $\mu g \cdot m^{-3}$ in spring, summer, autumn, and winter respectively. The SOA

542 concentrations in I/SVOC-E simulation were 2.4−3.6 times higher than those in BASE

543 simulation, which was 40% to 72% of the observation, indicating the large contributions

544 of I/SVOCs emissions to SOA production.

545 The I/SVOC-E simulation also demonstrated improvements in reproducing the

546 temporal variations of SOA, especially during the daytime (Figure 7e−7h). Compared

547 with the BASE simulation, evident increases in SOA concentrations during daytime can

548 be observed in I/SVOC-E simulation (Figure 7e−7h), which agrees better with the

549 observation. However, the model is still hard to capture the diurnal patterns of SOA

550 observed in most seasons, except for the summer, when both the concentrations and

551 diurnal variations of SOA are well reproduced, which indicates that SOA in summer is

552 mainly subject to photochemical oxidation of I/SVOC emissions, while SOA formation

will be largely affected by other factors in other seasons, especially during the nighttime in cool seasons. For example, an increasing body of experimental and observational evidence suggest that heterogeneous and multiphase reactions also played important roles in SOA formation especially during pollution episodes (Guo et al., 2020; Kim et al., 2022). Recent studies also found that nocturnal NO_3 oxidation was also an important route for SOA formation, which would drive the enhancement of SOA during the nighttime (Yu et al., 2019; Decker et al., 2021). Yet mechanism and parameterizations of these processes remain unclear, making the involvement of these processes in the model difficult. A recent study furtherly found that there were considerable emissions of condensable organic aerosols from stationary sources in the industrial and energy sectors, which would effectively improve the contributions of the industrial sector to OA simulation especially in winter, should also be considered in the future (Morino, et al., 2018; Morino, et al., 2022). In addition, I/SVOC emissions from outside of the YRD region might be underestimated due to the lack of detailed base emission inventory, resulting in the corresponding underestimation of the transported SOA, which were prominent especially in autumn, winter and spring in Shanghai. High-resolution I/SVOCs emissions inventory is urgently needed to be developed at a larger regional scale.
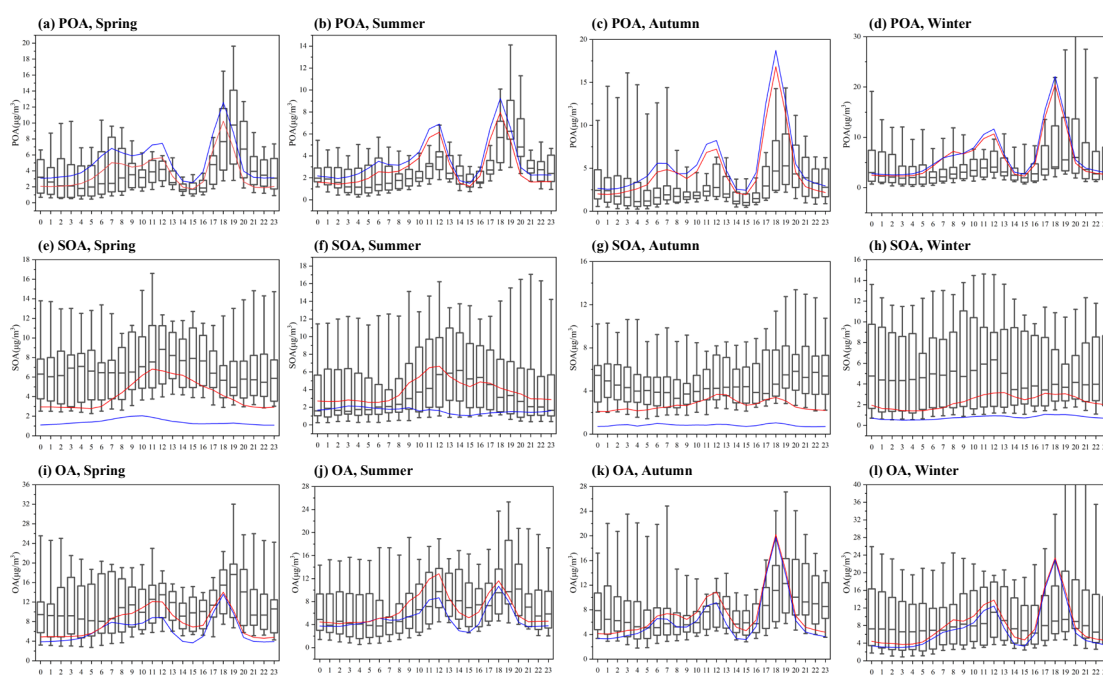
3.3 OA source contributions

3.3.1 POA and SOA sources in the region

Based on the high-resolution I/SVOC emission inventory established in this study, we successfully simulated the POA and SOA concentrations from each source. Table 3 summarizes the regional average concentrations of POA and SOA originated from different sources and their relative contributions. Residential POA dominated the regional OA, with average concentrations ranged from 1. 6 to 2.4 $\mu g \cdot m^{-3}$ in different seasons, accounting for 19.5%−25.3% of the total OA, among which cooking emission is the dominant source (*ca.* 98%) of residential POA. Other POA sources include industrial, biomass burning, and mobile sources, accounting for 8.0%−8.6%, 4. 5%−8.3%, and 5.0%−5.8% of the total OA, respectively. The cumulative fraction of POA in total OA from industrial and mobile sources was 13.4%−14.4%, close to that of HOA (15%) observed by the AMS measurement in Shanghai (Figure S5).

Industrial sources were the main source of SOA in the YRD region, with average SOA concentrations of 0.8−1.2 $\mu g \cdot m^{-3}$ in four seasons, accounting for 9.0%−15.6% of the total OA, among which, industrial process and solvent-use sources had almost equal contributions. Mobile sources were the second largest source of SOA in this region, with an average concentration of 0.3−0.5 $\mu g \cdot m^{-3}$, accounting for 3.4%−6.7% of the total OA. Among them, the source contribution of gasoline vehicles to SOA was 1.8%−3.1%, and that of diesel vehicles was 1.2%−2.6%. BVSOA showed significant seasonal differences with concentrations of 0.9, 1.3, 0.7, and 0.1 $\mu g \cdot m^{-3}$, respectively in spring, summer, autumn, and winter, accounting for 9.6%, 16.9%, 7.6%, and 1.2% of the total OA.

Overall, cooking emission was the major source of POA in YRD, accounting for 19.1%−25.0% of the total OA, which is consistent with our observations in Shanghai

26

601 (Huang et al., 2021a; Zhu et al., 2021). Both simulations and observations demonstrated

602 higher contributions of cooking emission in urban China than those reported overseas

603 (17%–18%) (Chen et al., 2021), which is attributed to the difference between Asian-

604 style and Western-style cooking. The results emphasize that cooking emission has

605 become a non-negligible source of non-fossil carbon in urban areas in eastern China.

606 Contributions from industrial sources were running the second among all sources,

607 accounting for 17.0%−24.1% of OA and 24.7%–26.8% of SOA, which is attributed to

608 the high I/SVOC emissions from industrial sources and is consistent with previous

609 studies (Miao et al., 2021). Other sources mainly include mobile sources (8.8% to 11.7%

610 of OA) and biomass burning (5.2%−8.9% of OA). Specifically, diesel and gasoline

611 vehicles were the major contributors among mobile sources, with higher contribution

612 from the former (4.0%−4.7%) than the latter (3.1%−4.0%), followed by diesel

613 machinery (1.3%−2.1%) and marine vessels (0.4%−0.9%). The contribution of biomass

614 burning was highest in winter (8.9%) compared to contributions of 5.2%−7.3% in other

615 seasons and it was even higher than contribution of mobile sources (8.76%) in winter.

616 The remaining 14.5%−35.6% of OA was from super region scale, which represented

617 OA originated from emissions outside the YRD region. Our results were generally

618 similar with those of Chang et al. (2022) for the YRD region. We both found the

619 domestic combustion mainly engaged in cooking emissions had a major contribution to

620 OA. Next was volatile chemical products (VCPs), especially the use of solvents, paints,

621 and adhesives in industrial sector, also made a high contribution. Note that industrial

622 process also took up a high fraction in our OA simulation, while it was lower in Chang

623 et al. (2022)'s study. The difference in I/SVOC emission estimates was the main reason

624 for this divergence. Mobile sources in both studies had similar contributions, which

625 accounted for about 10% to total OA. Comparatively, our source classification was

626 more specific, which will help identify more specific OA sources to design more refined

627 regional control countermeasures.

628 **Table 3.** POA and SOA source contributions of different emission sources in each season in the
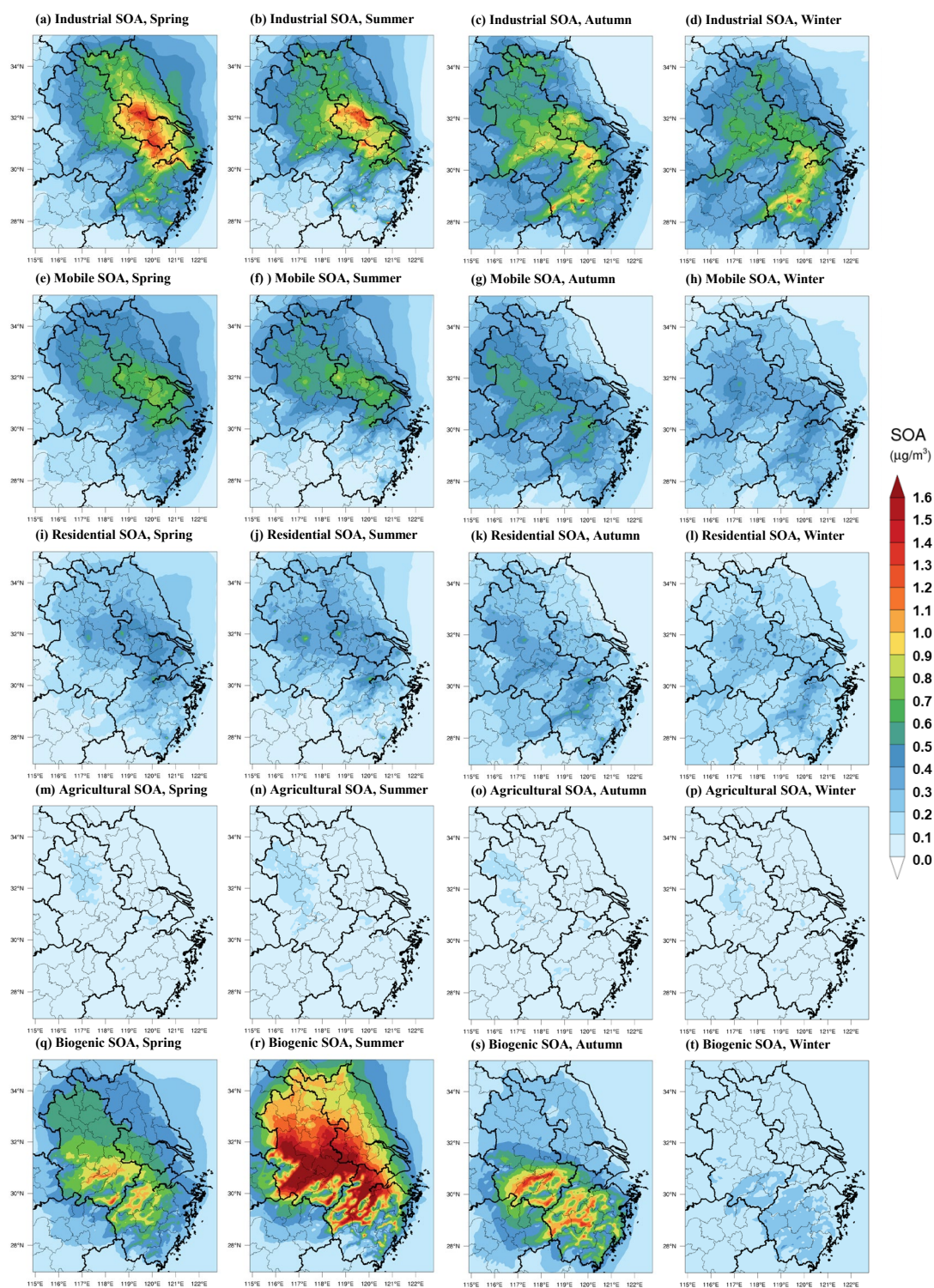
629   YRD region.

Sources	Spring conc. (µg·m⁻³)	Spring ratio (%)	Summer conc. (µg·m⁻³)	Summer ratio (%)	Autumn conc. (µg·m⁻³)	Autumn ratio (%)	Winter conc. (µg·m⁻³)	Winter ratio (%)
POA	4.5	49.2	3.1	41.7	5.1	55.1	6.0	64.3
Industrial sources	0.7	8.0	0.6	8.5	0.8	8.6	0.8	8.0
Industrial process	0.6	6.7	0.5	7.3	0.7	7.3	0.6	6.8
Industrial solvent-use	0.1	1.3	0.1	1.2	0.1	1.3	0.1	1.3
Mobile sources	0.5	5.4	0.4	5.0	0.5	5.8	0.5	5.4
Gasoline Vehicles	0.1	1.0	0.1	1.0	0.1	1.32	0.12	1.28
Diesel Vehicles	0.2	2.6	0.2	2.2	0.3	2.8	0.3	2.8
Diesel machinery	0.1	1.1	0.1	1.2	0.1	1.1	0.1	1.0
Marine vessel	0.1	0.8	0.1	0.7	0.1	0.6	0.0	0.4
Residential sources	1.8	19.5	1.6	21.0	2.3	25.3	2.4	25.2
Cooking	1.7	19.1	1.5	20.7	2.3	25.0	2.3	24.8
Other residential	0.03	0.3	0.02	0.2	0.03	0.3	0.04	0.4
Biomass burning	0.6	6.7	0.3	4.5	0.6	6.6	0.8	8.3
Super region	0.9	9.6	0.2	2.8	0.8	8.8	1.6	17.4
SOA	4.6	50.8	4.3	58.4	4.1	44.9	3.3	35.7
Industrial sources	1.2	13.4	1.2	15.6	1.0	11.1	0.8	9.0
Industrial process	0.7	7.5	0.6	8.4	0.6	6.6	0.5	5.6
Industrial solvent-use	0.5	5.8	0.5	7.3	0.4	4.5	0.3	3.3
Mobile sources	0.5	5.5	0.5	6.7	0.4	4.6	0.3	3.4
Gasoline Vehicles	0.3	2.7	0.2	3.1	0.2	2.3	0.2	1.8
Diesel Vehicles	0.2	2.0	0.2	2.5	0.2	1.7	0.1	1.2
Diesel machinery	0.1	0.7	0.1	0.9	0.1	0.6	0.03	0.4
Marine vessel	0.01	0.1	0.02	0.2	0.01	0.10	0.00	0.04
Residential sources	0.4	4.7	0.5	6.5	0.4	4.7	0.3	3.4
Cooking	0.2	2.3	0.3	4.0	0.3	2.8	0.2	1.7
Other residential	0.2	2.3	0.2	2.6	0.2	1.9	0.2	1.7
Biomass burning	0.1	0.6	0.1	0.7	0.1	0.6	0.1	0.6
Biogenic	0.9	9.6	1.3	16.9	0.7	7.6	0.1	1.2
Super region	1.6	17.0	0.9	11.8	1.5	16.3	1.7	18.2

630   3.3.2 Spatial distributions of SOA originated from different sources

631   Figure 8 shows the spatial distributions of modeled SOA originated from different

632   sources in each season in YRD region. Note that we only considered the SOA formed

633   from the intraregional VOC and I/SVOC emissions, excluding those transported from

634   the super region. A large spatial variability was observed for the sources of SOA driven

635   by emissions. For example, industrial and mobile SOA concentrated in the eastern and

636   central YRD, where I/SVOC emissions were high (Figure 4). Residential and

637   agricultural SOA presented a more uniform spatial distribution than industrial and

638   mobile SOA, with enhanced formation in central and western YRD (Figures 8i-8l).

639   Although absolute source-dependent SOA concentrations differ in different

640   seasons, low spatial variabilities were observed for different seasons. Industrial, mobile,

641   and residential sources were the predominant contributors to SOA formation in eastern

642   and central YRD, especially for the area along the Hangzhou Bay and Yangtze River

643   driven by the enhanced I/SVOC emissions. The spatial distributions of BVSOA have

644   been discussed above and will not be detailed here.

Figure 8. Spatial distributions of modeled SOA concentrations from different sources in each season in YRD region.

3.3.3 Predominant OA sources in sub-regions of YRD

To characterize the source contributions in different parts of the region, we categorized the simulation region into six sub-regions: northern YRD, western YRD,

651   central YRD, eastern YRD and southern YRD. And six representative cities in theses

652   six regions were further selected for detailed comparison in source contributions,

653   including Xuzhou (XZ), Hefei (HF), Nanjing (NJ), Hangzhou (HZ), Shanghai (SH) and

654   Jinhua (JH). Figure 9 shows their locations and OA source contributions during summer
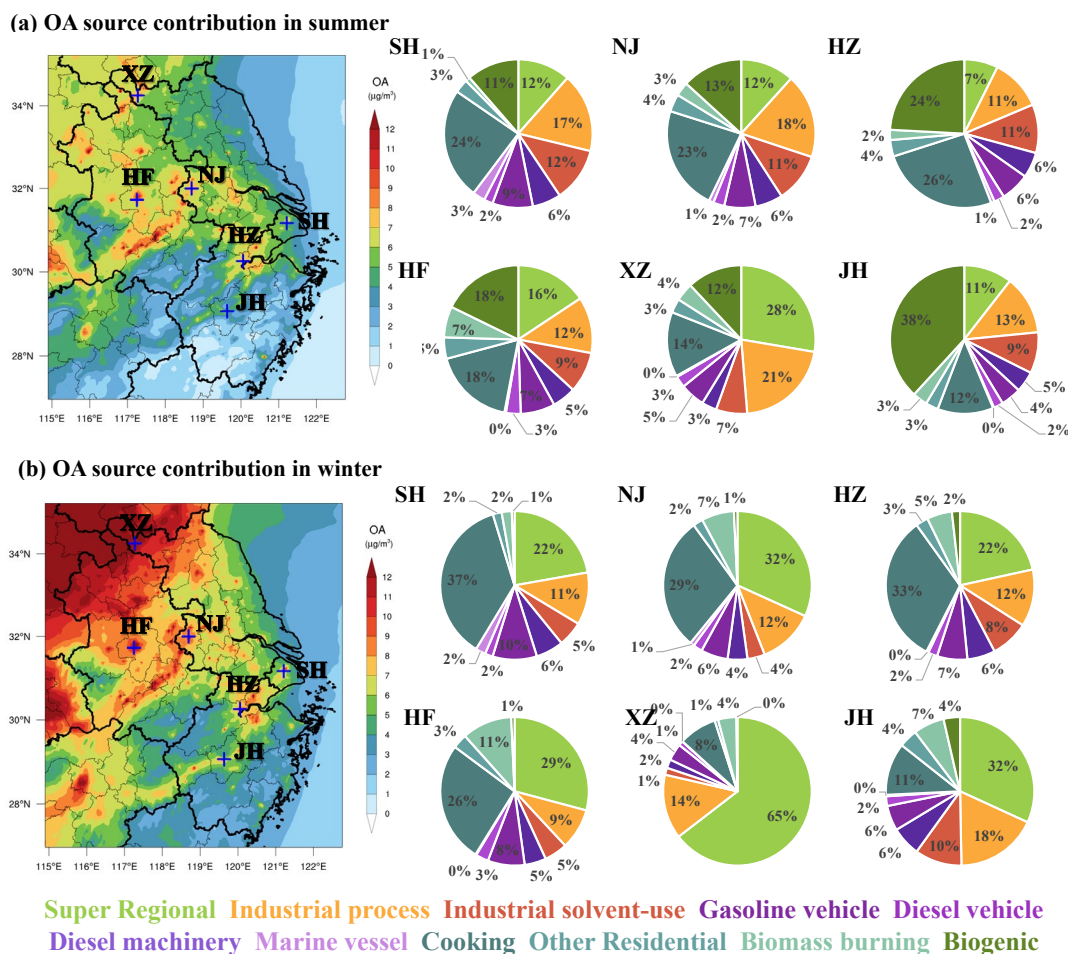
655   and winter.

656   In Northern YRD, represented by XZ, enhanced contribution from super-regional

657   scale to the local OA was observed for both winter (64.6%) and summer (27.7%) and

658   the contributions from industrial processes (14.0% in winter and 21.0% in summer)

659   were also higher than other sub-regions. Other major sources include biogenic (12.0%)

660   and cooking emissions (14.1%) in summer and cooking (8.3%) in winter. Taken

661   together, super-regional transportation and industrial processes are predominant

662   contributors of OA in northern YRD, accounting for 78.6% and 48.7% in summer and

663   winter respectively, followed by cooking emissions.

664   In western YRD, represented by HF, cooking emission was the largest contributor

665   to OA with contributions of 17.8% and 26.3% in both summer and winter respectively,

666   followed by super-regional contributions of 15.7% (summer) and 29.2% (winter). Other

667   major sources also include mobile source of 15.5%, biogenic source in summer (17.8%)

668   and industrial processes in both summer (12.3%) and winter (8.9%). In central YRD,

669   represented by NJ and HZ, the relative source contributions were very similar to those

670   in western YRD, with predominant contributions from cooking (22.8%-32.6%),

671   followed by super-regional transportation (7.4%-31.8%), industrial processes (11.3%-

672   18.4%) and mobile source (13.1%-16.3%).

673   In eastern YRD, represented by SH, the largest OA source was cooking emission,

674   account for 24.3% and 36.6% of OA in summer and winter respectively, followed by

675   mobile sources of 19%, super-regional transportation of 11.5% (summer) and 22.2%

676   (winter) and industrial processes of 17.3% (summer) and 11.4% (winter). In southern

677   YRD, represented by JH, while biogenic contribution was prevailing in summer

678   (38.2%), super-regional transportation was significant in winter (31.8%). Similar to

679   other sub-regions, other major sources also included the contributions of cooking

680   emission of 12.2% (summer) and 11.4% (winter), industrial processes of 12.9%

681   (summer) and 17.9% (winter) and mobile sources of 13%. Yet southern YRD presented

682   more evident increase in the contribution from industrial solvent-use compared with

683   other sub-regions.

684   To summarize, cooking, super-regional transportation, industrial process and mobile

685   sources were the predominant sources of OA in all sub-regions regardless of the season,

686   albeit enhanced contributions from biogenic sources to the OA formation in summer

687   was observed, especially in southern YRD. High contributions of cooking sources were

688   in accordance with the distributions of populations and high contributions of mobile

689   sources were somewhat expected, especially in the city centers. Source contributions of

690   OA varies in the intraregional scale implies that more targeted control measures need

691   to be designed according to the emission features of each city. Specifically, for densely

692   populated area, it is necessary to strengthen the future control strategy of cooking

693   emissions; special attention needs to be paid to the I/SVOC emissions from industrial

694   sources in eastern, central, and northern YRD region; mobile sources show its

695   significance in urban aera of the region, dominated by the equal contributions from

696   gasoline and diesel vehicles, indicating further reductions on the I/SVOCs from vehicle

697   emissions are therefore critical for pollution control on city scale.

(a) OA source contribution in summer

(b) OA source contribution in winter

Super Regional Industrial process Industrial solvent-use Gasoline vehicle Diesel vehicle Diesel machinery Marine vessel Cooking Other Residential Biomass burning Biogenic

Figure 9. Source contributions of modeled OA concentrations from different sources during summer and winter in different cities of the region.

4. Conclusions

In this study, we established a high-resolution I/SVOC emission inventory with detailed source profiles and applied it into CMAQ v5.3 to simulate POA and SOA formation in YRD region of China. With the addition of I/SVOC emissions, simulation results show significant improvements on both temporal variations and spatial distributions of OA. Compared with the BASE simulation, where I/SVOC emissions were not included, the simulated SOA increased by 1.5 times in I/SVOC-E simulation, highlighting the significant contributions of I/SVOC emissions to SOA production. The remaining 10%−30% underestimation of OA indicates that future work is still needed in bridging the gap between simulation and observations, such as, measuring local emission factors and source profiles of I/SVOC from various local sources, updating

712   SOA formation mechanisms in model framework.

713   With the addition of source specific I/SVOC emissions, we successfully quantified

714   the contribution of each source to POA and SOA concentrations in YRD. For POA,

715   cooking emission is the predominant source, which concentrates in urban area of YRD

716   in accordance with the population distribution. For SOA, for the first time, we

717   demonstrate that I/SVOCs from industrial sources are dominant contributor, followed

718   by those from mobile sources. In summer, the contributions of biogenic emission to

719   total SOA are also non-negligible, especially for the cities in southern YRD. Spatial and

720   seasonal variations in the source contributions suggest that control strategies for OA

721   pollution should vary by cities and seasons. For urban area, cooking emissions has been

722   emerging as an important POA source, not to mention their impacts on SOA formation

723   are not yet certain. Our results suggest the control measures on the cooking emissions

724   should be strengthened in the future for the further reduction of POA. Another

725   important source of SOA in urban area is mobile source, especially gasoline and diesel

726   vehicles. Reduction in I/SVOC emissions from vehicles are effective measures in the

727   mitigation of urban air pollution, which is also technically feasible as has been

728   demonstrated in Qi et al. (2021). Continuous improvement in emission standards is one

729   way to promote the reduction of motor vehicle related SOA. Our study further reveals

730   that non-tailpipe sources of I/SVOCs (e.g., solvent use, petrochemical, etc.) are major

731   contributors to SOA formation in the YRD region, consistent with Chang et al. (2022)'s

732   model results in the national scale. However, current understanding of SOA formation

733   potentials from these sources are still far from enough. For example, the localized

734   I/SVOC emission factors and source profiles of these sources are still missing. Their

735   chemical behavior and SOA yields may be different from the emissions from mobile

736   sources which have been widely studied, which urges in-depth studies on these sources

737   as well as the corresponding control measures.

738   *Data availability*

739   The gridded emissions of I/SVOCs from various sources for the YRD region

developed by this study at a horizontal resolution of 4 km × 4 km can be downloaded from the following website (https://doi.org/10.6084/m9.figshare.19536082.v1). Additional related data are available upon request by contacting the corresponding author (Cheng Huang; huangc@saes.sh.cn).

Supplement

The supplement related to this article is available online.

Author contributions

CH, JA, DH, and MQ designed the research. CH and JA developed the I/SVOC emission inventory. JA, MQ, and RY performed the model. DH, LQ, MZ, YL, SZ, and QW collected the observation data. CH, JA, DH, and HW analyzed the results. CH, JA, and DH wrote the paper.

Competing interests

The authors declare that they have no conflict of interest.

References

An, J., Huang, Y., Huang, C., Wang, X., Yan, R., Wang, Q., Wang, H., Jing, S., Zhang, Y., Liu, Y., Chen, Y., Xu, C., Qiao, L., Zhou, M., Zhu, S., Hu, Q., Lu, J., and Chen, C.: Emission

767   inventory of air pollutants and chemical speciation for specific anthropogenic sources

768   based on local measurements in the Yangtze River Delta region, China, Atmos. Chem.

769   Phys., 21, 2003–2025, 2021.

770 Boylan, J. W., and Russell, A. G.: PM and light extinction model performance metrics, goals,

771   and criteria for three-dimensional air quality models, Atmos. Environ., 40, 4946–4959,

772   2006.

773 Cai, S., Zhu, L., Wang, S., Wisthaler, A., Li, Q., Jiang, J., and Hao, J.: Time-resolved

774   intermediate-volatility and semivolatile organic compound emissions from household coal

775   combustion in northern China, Environ. Sci. Technol., 53, 9269−9278, 2019.

776 Canagaratna, M. R., Jayne, J. T., Jimenez, J. L., Allan, J. D., Alfarra, M. R., Zhang, Q., Onasch,

777   T. B., Drewnick, F., Coe, H., Middlebrook, A., Delia, A., Williams, L. R., Trimborn, A. M.,

778   Northway, M. J., DeCarlo, P. F., Kolb, C. E., Davidovits, P., and Worsnop, D. R.: Chemical

779   and microphysical characterization of ambient aerosols with the aerodyne aerosol mass

780   spectrometer, Mass Spectrom. Rev., 26, 185−222, 2007.

781 Canonaco, F., Crippa, M., Slowik, J. G., Baltensperger, U., and Prévôt, A. S. H.: SoFi, an IGOR-

782   based interface for the efficient use of the generalized multilinear engine (ME-2) for the

783   source apportionment: ME-2 application to aerosol mass spectrometer data, Atmos. Meas.

784   Tech., 6, 3649–3661, 2013.

785 Chang, X., Zhao, B., Zheng, H., Wang, S., Cai, S., Guo, F., Gui, P., Huang, G., Wu, D., Han, L.,

786   Xing, J., Man, H., Hu, R., Liang, C., Xu, Q., Qiu, X., Ding, D., Liu, K., Han, R., Robinson,

787   A. L., and Donahue, N. M.: Full-volatility emission framework corrects missing and

788   underestimated secondary organic aerosol sources, One Earth, 5, 403–412, 2022.

789 Chen, W., Ye, Y., Hu, W., Zhou, H., Pan, T., Wang, Y., Song, W., Song, Q., Ye, C., Wang, C.,

790   Wang, B., Huang, S., Yuan, B., Zhu, M., Lian, X., Zhang, G., Bi, X., Jiang, F., Liu, J.,

791   Canonaco, F., Prevot, A. S. H., Shao, M., and Wang, X.: Real-time characterization of

792   aerosol compositions, sources, and aging processes in Guangzhou during PRIDE-GBA

793   2018 campaign, J. Geophys. Res., Atmos., 126, e2021JD035114, 2021.

794 Crippa, M., Canonaco, F., Lanz, V. A., Äijälä, M., Allan, J. D., Carbone, S., Capes, G., Ceburnis,

795   D., Dall'Osto, M., Day, D. A., DeCarlo, P. F., Ehn, M., Eriksson, A., Freney, E.,

796   Hildebrandt Ruiz, L., Hillamo, R., Jimenez, J. L., Junninen, H., Kiendler-Scharr, A.,

797   Kortelainen, A. M., Kulmala, M., Laaksonen, A., Mensah, A. A., Mohr, C., Nemitz, E.,

798   O'Dowd, C., Ovadnevaite, J., Pandis, S. N., Petäjä, T., Poulain, L., Saarikoski, S., Sellegri,

799   K., Swietlicki, E., Tiitta, P., Worsnop, D. R., Baltensperger, U., and Prévôt, A. S. H.:

800   Organic aerosol components derived from 25 AMS data sets across Europe using a

801   consistent ME-2 based source apportionment approach, Atmos. Chem. Phys., 14, 6159–

802   6176, 2014.

803 Cross, E. S., Hunter, J. F., Carrasquillo, A. J., Franklin, J. P., Herndon, S. C., Jayne, J. T.,

804   Worsnop, D. R., Miake-Lye, R. C., and Kroll, J. H.: Online measurements of the emissions

805   of intermediate-volatility and semi-volatile organic compounds from aircraft, Atmos.

806   Chem. Phys., 13, 7845–7858, 2013.

807 Decker, Z. C. J., Robinson, M. A., Barsanti, K. C., Bourgeois, I., Coggon, M. M., DiGangi, J.

808   P., Diskin, G. S., Flocke, F. M., Franchin, A., Fredrickson, C. D., Gkatzelis, G. I., Hall, S.

809   R., Halliday, H., Holmes, C. D., Gregory Huey, L., Lee, Y. R., Lindaas, J., Middlebrook,

810   A. M., Montzka, D. D., Moore, R., Andrew Neuman, J., Nowak, J. B, Palm, B. B., Peischl,

811   J., Piel, F., Rickly, P. S., Rollins, A. W., Ryerson, T. B., Schwantes, R. H., Sekimoto, K.,

812   Thornhill, L., Thornton, J. A., Tyndall, G. S., Ullmann, K., Van Rooy, P., Veres, P. R.,

813   Warneke, C., Washenfelder, R. A., Weinheimer, A. J., Wiggins, E., Winstead, E., Wisthaler,

814   A., Womack, C., and Brown, S. S.: Nighttime and daytime dark oxidation chemistry in

815   wildfire plumes: an observation and model analysis of FIREX-AQ aircraft data, Atmos.

816   Chem. Phys., 21, 16293–16317, 2021.

817 Donahue, N. M., Robinson, A. L., and Pandis, S. N.: Atmospheric organic particulate matter:

818   From smoke to secondary organic aerosol, Atmos. Environ., 43, 94–106, 2009.

819 Donahue, N. M., Robinson, A. L., Stanier, C. O., and Pandis, S. N.: Coupled Partitioning,

820   Dilution, and Chemical Aging of Semivolatile Organics, Environ. Sci. Technol., 40, 2635–

821   2643, 2006.

822 Drozd, G. T., Weber, R. J., and Goldstein, A. H.: Highly resolved composition during diesel

823   evaporation with modeled ozone and secondary aerosol formation: Insights into pollutant

824   formation from evaporative intermediate volatility organic compound sources, Environ.

825   Sci. Technol., 55, 5742−5751, 2021.

826 Drozd, G. T., Zhao, Y., Saliba, G., Frodin, B., Maddox, C., Oliver Chang, M.-C., Maldonado,

827   H., Sardar, S., Weber, R. J., Robinson, A. L., and Goldstein, A. H.: Detailed speciation of

828   intermediate volatility and semivolatile organic compound emissions from gasoline

829   vehicles: Effects of cold-starts and implications for secondary organic aerosol formation,

830   Environ. Sci. Technol., 53, 1706–1714, 2019.

831 Emery, C., Tai, E., and Yarwood, G.: Enhanced meteorological modeling and performance

832   evaluation for two Texas ozone episodes, Prepared for the Texas natural resource

833   conservation commission, by ENVIRON International Corporation, 2001.

834 Gentner, D. R., Isaacman, G., Worton, D. R., Chan, A. W. H., Dallmann, T. R., Davis, L., Liu,

835   S., Day, D. A., Russell, L. M., Wilson, K. R., Weber, R., Guha, A., Harley, R. A., and

836   Goldstein, A. H.: Elucidating secondary organic aerosol from diesel and gasoline vehicles

837   through detailed characterization of organic carbon emissions, Proc. Natl. Acad. Sci., 109,

838   18318−18323, 2012.

839 Guo, J., Zhou, S., Cai, M., Zhao, J., Song, W., Zhao, W., Hu, W., Sun, Y., He, Y., Yang, C., Xu,

840   X., Zhang, Z., Cheng, P., Fan, Q., Hang, J., Fan, S., Wang, X., and Wang, X.:

841   Characterization of submicron particles by time-of-flight aerosol chemical speciation

842   monitor (ToF-ACSM) during wintertime: aerosol composition, sources, and chemical

843   processes in Guangzhou, China, Atmos. Chem. Phys., 20, 7595–7615, 2020.

844 Hallquist, M., Wenger, J. C., Baltensperger, U., Rudich, Y., Simpson, D., Claeys, M., Dommen,

845   J., Donahue, N. M., George, C., Goldstein, A. H., Hamilton, J. F., Herrmann, H., Hoffmann,

846   T., Iinuma, Y., Jang, M., Jenkin, M. E., Jimenez, J. L., Kiendler-Scharr, A., Maenhaut, W.,

847   McFiggans, G., Mentel, Th. F., Monod, A., Prévôt, A. S. H., Seinfeld, J. H., Surratt, J. D.,

848   Szmigielski, R., and Wildt, J.: The formation, properties and impact of secondary organic

849   aerosol: Current and emerging issues, Atmos. Chem. Phys., 9, 5155–5236, 2009.

850 Hayes, P. L., Ortega, A. M., Cubison, M. J., Froyd, K. D., Zhao, Y., Cliff, S. S., Hu, W. W.,

Toohey, D. W., Flynn, J. H., Lefer, B. L., Grossberg, N., Alvarez, S., Rappenglück, B., Taylor, J. W., Allan, J. D., Holloway, J. S., Gilman, J. B., Kuster, W. C., de Gouw, J. A., Massoli, P., Zhang, X., Liu, J., Weber, R. J., Corrigan, A. L., Russell, L. M., Isaacman, G., Worton, D. R., Kreisberg, N. M., Goldstein, A. H., Thalman, R., Waxman, E. M., Volkamer, R., Lin, Y. H., Surratt, J. D., Kleindienst, T. E., Offenberg, J. H., Dusanter, S., Griffith, S., Stevens, P. S., Brioude, J., Angevine, W. M., and Jimenez, J. L.: Organic aerosol composition and sources in Pasadena, California, during the 2010 CalNex campaign, J. Geophys. Res., Atmos., 118, 9233–9257, 2013.

Huang, C., Hu, Q., Li, Y., Tian, J., Ma, Y., Zhao, Y., Feng, J., An, J., Qiao, L., Wang, H., Jing, S., Huang, D., Lou, S., Zhou, M., Zhu, S., Tao, S., and Li, L.: Intermediate volatility organic compound emissions from a large cargo vessel operated under real-world conditions, Environ. Sci. Technol., 52, 12934–12942, 2018.

Huang, D., Zhu, S., An, J., Wang, Q., Qiao, L., Zhou, M., He, X., Ma, Y., Sun, Y., Huang, C., Yu, J., and Zhang, Q.: Comparative assessment of cooking emission contributions to urban organic aerosol using online molecular tracers and aerosol mass spectrometry measurements, Environ. Sci. Technol., 55, 14526–14535, 2021a.

Huang, L., Wang, Q., Wang, Y., Emery, C., Zhu, A., Zhu, Y., Yin, S., Yarwood, G., Zhang, K., and Li, L.: Simulation of secondary organic aerosol over the Yangtze River Delta region: The impacts from the emissions of intermediate volatility organic compounds and the SOA modeling framework, Atmos. Environ., 246, 118079, 2021b.

Huang, R. J., Zhang, Y., Bozzetti, C., Ho, K., Cao, J., Han, Y., Daellenbach, K. R., Slowik, J. G., Platt, S. M., Canonaco, F., Zotter, P., Wolf, R., Pieber, S. M., Bruns, E. A., Crippa, M., Ciarelli, G., Piazzalunga, A., Schwikowski, M., Abbaszade, G., Schnelle-Kreis, J., Zimmermann, R., An, Z., Szidat, S., Baltensperger, U., El Haddad, I., and Prévôt, A. S. H.: High secondary aerosol contribution to particulate pollution during haze events in China, Nature, 514, 218–222, 2014.

Huffman, J., Docherty, K., Mohr, C., Cubison, M., Ulbrich, I., Ziemann, P., Onasch, T., and Jimenez, J.: Chemically-resolved volatility measurements of organic aerosol from

879   different sources, Environ. Sci. Technol., 43, 5351–5357, 2009.

880   Jathar, S. H., Gordon, T. D., Hennigan, C. J., Pye, H. O. T., Pouliot, G., Adams, P. J., Donahue,

881   N. M., and Robinson, A. L.: Unspeciated organic emissions from combustion sources and

882   their influence on the secondary organic aerosol budget in the United States, P. Natl. Acad.

883   Sci. USA, 111, 10473–10478, 2014.

884   Jathar, S. H., Woody, M., Pye, H. O. T., Baker, K. R., and Robinson, A. L.: Chemical transport

885   model simulations of organic aerosol in southern California: model evaluation and

886   gasoline and diesel source contributions, Atmos. Chem. Phys., 17, 4305–4318, 2017.

887   Jimenez, J. L., Canagaratna, M. R., Donahue, N. M., Prevot, A. S. H., Zhang, Q., Kroll, J. H.,

888   DeCarlo, P. F., Allan, J. D., Coe, H., Ng, N. L., Aiken, A. C., Docherty, K. S., Ulbrich, I.

889   M., Grieshop, A. P., Robinson, A. L., Duplissy, J., Smith, J. D., Wilson, K. R., Lanz, V. A.,

890   Hueglin, C., Sun, Y. L., Tian, J., Laaksonen, A., Raatikainen, T., Rautiainen, J., Vaattovaara,

891   P., Ehn, M., Kulmala, M., Tomlinson, J. M., Collins, D. R., Cubison, M. J., Dunlea, J.,

892   Huffman, J. A., Onasch, T. B., Alfarra, M. R., Williams, P. I., Bower, K., Kondo, Y.,

893   Schneider, J., Drewnick, F., Borrmann, S., Weimer, S., Demerjian, K., Salcedo, D., Cottrell,

894   L., Griffin, R., Takami, A., Miyoshi, T., Hatakeyama, S., Shimono, A., Sun, J. Y., Zhang,

895   Y. M., Dzepina, K., Kimmel, J. R., Sueper, D., Jayne, J. T., Herndon, S. C., Trimborn, A.

896   M., Williams, L. R., Wood, E. C., Middlebrook, A. M., Kolb, C. E., Baltensperger, U., and

897   Worsnop, D. R.: Evolution of Organic Aerosols in the Atmosphere, Science, 326, 1525–

898   1529, 2009.

899   Kim, D., Cho, C., Jeong, S., Lee, S., Nault, B. A., Campuzano-Jost, P., Day, D. A., Schroder, J.

900   C., Jimenez, J. L., Volkamer, R., Blake, D. R., Wisthaler, A., Fried, A., DiGangi, J. P.,

901   Diskin, G. S., Pusede, S. E., Hall, S. R., Ullmann, K., Gregory Huey, L., Tanner, D. J.,

902   Dibb, J., Knote, C. J., and Min, K., Field observational constraints on the controllers in

903   glyoxal (CHOCHO) reactive uptake to aerosol, Atmos. Chem. Phys., 22, 805–821, 2022.

904   Kim, Y., Couvidat, F., Sartelet, K., and Seigneur, C.: Comparison of different gas-phase

905   mechanisms and aerosol modules for simulating particulate matter formation, J. Air Waste

906   Manage., 61, 1218–1226, 2011.

Koo, B., Knipping, E., and Yarwood, G.: 1.5-Dimensional volatility basis set approach for modeling organic aerosol in CAMx and CMAQ, Atmos. Environ., 95, 158–164, 2014.

Koss, A. R., Sekimoto, K., Gilman, J. B., Selimovic, V., Coggon, M. M., Zarzana, K. J., Yuan, B., Lerner, B. M., Brown, S. S., Jimenez, J. L., Krechmer, J., Roberts, J. M., Warneke, C., Yokelson, R. J., and de Gouw, J.: Non-methane organic gas emissions from biomass burning: identification, quantification, and emission factors from PTR-ToF during the FIREX 2016 laboratory experiment, Atmos. Chem. Phys., 18, 3299–3319, 2018.

Li, J., Cao, L., Gao, W., He, L., Yan, Y., He, Y., Pan, Y., Ji, D., Liu, Z., and Wang, Y.: Seasonal variations in the highly time-resolved aerosol composition, sources and chemical processes of background submicron particles in the North China Plain, Atmos. Chem. Phys., 21, 4521–4539, 2021.

Li, J., Han, Z., Li, J., Liu, R., Wu, Y., Liang, L., and Zhang, R.: The formation and evolution of secondary organic aerosol during haze events in Beijing in wintertime, Sci. Total Environ., 703, 134937, 2020.

Li, J., Han, Z., Wu, J., Tao, J., Li, J., Sun, Y., Liang, L., Liang, M., and Wang, Q.: Secondary organic aerosol formation and source contributions over east China in summertime, Environ. Pollut., 306, 119383, 2022.

Li, M., Zhang, Q., Kurokawa, J. i., Woo, J. H., He, K., Lu, Z., Ohara, T., Song, Y., Streets, D. G., Carmichael, G. R., Cheng, Y., Hong, C., Huo, H., Jiang, X., Kang, S., Liu, F., Su, H., Zheng, B.: MIX: a mosaic Asian anthropogenic emission inventory under the international collaboration framework of the MICS-Asia and HTAP. Atmos. Chem. Phys., 17, 935–963, 2017.

Li, Y., Ren, B., Qiao, Z., Zhu, J., Wang, H., Zhou, M., Qiao, L., Lou, S., Jing, S., Huang, C., Tao, S., Rao, P., and Li, J.: Characteristics of atmospheric intermediate volatility organic compounds (IVOCs) in winter and summer under different air pollution levels, Atmos. Environ., 210, 58–65, 2019.

Li, Y. J., Sun, Y. L., Zhang, Q., Li, X., Li, M., Zhou, Z., and Chan, C. K.: Real-time chemical characterization of atmospheric particulate matter in China: A review, Atmos. Environ.,

158, 270–304, 2017.

Liggio, J., Li, S., Hayden, K., Taha, Y. M., Stroud, C., Darlington, A., Drollette, B. D., Gordon, M., Lee, P., Liu, P., Leithead, A., Moussa, S. G., Wang, D., Brien, J. O., Mittermeier, R. L., Osthoff, H. D., Makar, P. A., Zhang, J., Brook, J. R., Lu, G., Staebler, R. M., Han, Y., Travis, W., Plata, D. L., and Gentner, D. R.: Oil sands operations as a large source of secondary organic aerosols, Nature, 534, 1–16, 2016.

Ling, Z., Wu, L., Wang, Y., Shao, M., Wang, X., and Huang, W.: Roles of semivolatile and intermediate-volatility organic compounds in secondary organic aerosol formation and its implication: A review, J. Environ. Sci., 114, 259–285, 2022.

Liu, H., Man, H., Cui, H., Wang, Y., Deng, F., Wang, Y., Yang, X., Xiao, Q., Zhang, Q., Ding, Y., and He, K.: An updated emission inventory of vehicular VOCs and IVOCs in China, Atmos. Chem. Phys., 17, 12709–12724, 2017.

Liu, H., Meng, Z., Lv, Z., Wang, X., Deng, F., Liu, Y., Zhang, Y., Shi, M., Zhang, Q., and He, K.: Emissions and health impacts from global shipping embodied in US–China bilateral trade, Nat. Sustain., 2, 1027–1033, 2019.

Liu, Y., Li, L., An, J., Huang, L., Yan, R., Huang, C., Wang, H., Wang, Q., Wang, M., and Zhang, W.: Estimation of biogenic VOC emissions and its impact on ozone formation over the Yangtze River Delta region, China, Atmos. Environ., 186, 113–128, 2018a.

Liu, Z., Gao, W., Yu, Y., Hu, B., Xin, J., Sun, Y., Wang, L., Wang, G., Bi, X., Zhang, G., Xu, H., Cong, Z., He, J., Xu, J., and Wang, Y.: Characteristics of $PM_{2.5}$ mass concentrations and chemical species in urban and background areas of China: emerging results from the CARE-China network, Atmos. Chem. Phys., 18, 8849–8871, 2018b.

Louvaris, E. E., Florou, K., Karnezi, E., Papanastasiou, D. K., Gkatzelis, G. I., and Pandis, S. N.: Volatility of source apportioned wintertime organic aerosol in the city of Athens, Atmos. Environ., 158, 138–147, 2017.

Lu, Q., Murphy, B. N., Qin, M., Adams, P. J., Zhao, Y., Pye, H. O. T., Efstathiou, C., Allen, C., and Robinson, A. L.: Simulation of organic aerosol formation during the CalNex study: Updated mobile emissions and secondary organic aerosol parameterization for

963   intermediate-volatility organic compounds, Atmos. Chem. Phys., 20, 4313–4332, 2020.

964   Lu, Q., Zhao, Y., and Robinson, A. L.: Comprehensive organic emission profiles for gasoline,

965   diesel, and gas-turbine engines including intermediate and semi-volatile organic

966   compound emissions, Atmos. Chem. Phys., 18, 17637–17654, 2018.

967   May, A. A., Levin, E. J. T., Hennigan, C. J., Riipinen, I., Lee, T., Collett, J. L., Jimenez, J. L.,

968   Kreidenweis, S. M., and Robinson, A. L.: Gas-particle partitioning of primary organic

969   aerosol emissions: 3. Biomass burning, J. Geophys. Res.-Atmos., 118, 11327–11338, 2013.

970   McDonald, B. C., de Gouw, J. A., Gilman, J. B., Jathar, S. H., Akherati, A., Cappa, C. D.,

971   Jimenez, J. L., Lee-Taylor, J., Hayes, P. L., McKeen, S. A., Cui, Y. Y., Kim, S., Gentner,

972   D. R., Isaacman-VanWertz, G., Goldstein, A. H., Harley, R. A., Frost, G. J., Roberts, J. M.,

973   Ryerson, T. B., and Trainer, M.: Volatile chemical products emerging as largest

974   petrochemical source of urban organic emissions, Science, 359, 760–764, 2018.

975   Miao, R., Chen, Q., Shrivastava, M., Chen, Y., Zhang, L., Hu, J., Zheng, Y., and Liao, K.:

976   Process-based and observation-constrained SOA simulations in China: the role of

977   semivolatile and intermediate-volatility organic compounds and OH levels, Atmos. Chem.

978   Phys., 21, 16183–16201, 2021.

979   Ming, L., Jin, L., Li, J., Fu, P., Yang, W., Liu, D., Zhang, G., Wang, Z., and Li, X.: $PM_{2.5}$ in the

980   Yangtze River Delta, China: Chemical compositions, seasonal variations, and regional

981   pollution events, Environ. Pollut., 223, 200–212, 2017.

982   Morino, Y., Chatani, S., Tanabe, K., Fujitani, Y., Morikawa, T., Takahashi, K., Sato, K., and

983   Sugata, S.: Contributions of condensable particulate matter to atmospheric organic aerosol

984   over Japan, Environ. Sci. Technol., 52, 8456−8466, 2018.

985   Morino, Y., Chatani, S., Fujitani, Y., Tanabe, K., Murphy, B. N., Jathar, S. H., Takahashi, K.,

986   Sato, K., Kumagai, K., and Saito, S.: Emissions of condensable organic aerosols from

987   stationary combustion sources over Japan, Atmos. Environ., 289, 119319, 2022.

988   Murphy, B. N., Woody, M. C., Jimenez, J. L., Carlton, A. M. G., Hayes, P. L., Liu, S., Ng, N.

989   L., Russell, L. M., Setyan, A., and Xu, L.: Semivolatile POA and parameterized total

990   combustion SOA in CMAQv5.2: impacts on source strength and partitioning, Atmos.

991   Chem. Phys., 17, 11107–11133, 2017.

992   Nault, B. A., Jo, D. S., McDonald, B. C., Campuzano-Jost, P., Day, D. A., Hu, W., Schroder, J.

993   C., Allan, J., Blake, D. R., Canagaratna, M. R., Coe, H., Coggon, M. M., DeCarlo, P. F.,

994   Diskin, G. S., Dunmore, R., Flocke, F., Fried, A., Gilman, J. B., Gkatzelis, G., Hamilton,

995   J. F., Hanisco, T. F., Hayes, P. L., Henze, D. K., Hodzic, A., Hopkins, J., Hu, M., Huey, L.

996   G., Jobson, B. T., Kuster, W. C., Lewis, A., Li, M., Liao, J., Nawaz, M. O., Pollack, I. B.,

997   Peischl, J., Rappenglück, B., Reeves, C. E., Richter, D., Roberts, J. M., Ryerson, T. B.,

998   Shao, M., Sommers, J. M., Walega, J., Warneke, C., Weibring, P., Wolfe, G. M., Young, D.

999   E., Yuan, B., Zhang, Q., de Gouw, J. A., and Jimenez, J. L.: Secondary organic aerosols

1000   from anthropogenic volatile organic compounds contribute substantially to air pollution

1001   mortality, Atmos. Chem. Phys., 21, 11201–11224, 2021.

1002   Presto, A. A., Miracolo, M. A., Kroll, J. H., Worsnop, D. R., Robinson, A. L., and Donahue, N.

1003   M.: Intermediate-volatility organic compounds: A potential source of ambient oxidized

1004   organic aerosol, Environ. Sci. Technol., 43, 4744–4749, 2009.

1005   Presto, A. A., Nguyen, N. T., Ranjan, M., Reeder, A. J., Lipsky, E. M., Hennigan, C. J., Miracolo,

1006   M. A., Riemer, D. D., and Robinson, A. L.: Fine particle and organic vapor emissions from

1007   staged tests of an in-use aircraft engine, Atmos. Environ., 45, 3603–3612, 2011.

1008   Pye, H. O. T., Seinfeld, J. H.: A global perspective on aerosol from low-volatility organic

1009   compounds, Atmos. Chem. Phys., 10, 4377–4401, 2010.

1010   Qi, L., Liu, H., Shen, X., Fu, M., Huang, F., Man, H., Deng, F., Shaikh, A. A., Wang, X., Dong,

1011   R., Song, C., and He, K.: Intermediate-volatility organic compound emissions from

1012   nonroad construction machinery under different operation modes, Environ. Sci. Technol.,

1013   53, 13832–13840, 2019.

1014   Qi, L., Zhao, J., Li, Q., Su, S., Lai, Y., Deng, F., Man, H., Wang, X., Shen, X., Lin, Y., Ding, Y.,

1015   and Liu, H.: Primary organic gas emissions from gasoline vehicles in China: Factors,

1016   composition and trends, Environ. Pollut., 290, 117984, 2021.

1017   Qin, M., Hu, A., Mao, J., Li, X., Sheng, L., Sun, J., Li, J., Wang, X., Zhang, Y., Hu, J.: $PM_{2.5}$

1018   and O_3 relationships affected by the atmospheric oxidizing capacity in the Yangtze River

1019   Delta, China, Sci. Total Environ., 810, 152268, 2022.

1020 Ren, B., Zhu, J., Tian, L., Wang, H., Huang, C., Jing, S., Lou, S., An, J., Lu, J., Rao, P., Fu, Q.,

1021   Huo, J., and Li, Y.: An alternative semi-quantitative GC/MS method to estimate levels of

1022   airborne intermediate volatile organic compounds (IVOCs) in ambient air, Atmos.

1023   Environ., X6, 100075, 2020.

1024 Robinson, A. L., Donahue, N. M., Shrivastava, M. K., Weitkamp, E. A., Sage, A. M., Grieshop,

1025   A. P., Lane, T. E., Pierce, J. R., and Pandis, S. N.: Rethinking organic aerosols:

1026   Semivolatile emissions and photochemical aging, Science, 315, 1259–1262, 2007.

1027 Sartelet, K., Zhu, S., Moukhtar, S., André, M., Gros, V., Favez, O., Brasseurh, A., and Redaelli,

1028   M.: Emission of intermediate, semi and low volatile organic compounds from traffic and

1029   their impact on secondary organic aerosol concentrations over greater paris, Atmos.

1030   Environ, 180, 126–137, 2018.

1031 Shrivastava, M. K., Cappa, C. D., Fan, J., Goldstein, A. H., Guenther, A. B., Jimenez, J. L.,

1032   Kuang, C., Laskin, A., Martin, S. T., Ng, N. L., Petaja, T., Pierce, J. R., Rasch, P. J., Roldin,

1033   P., Seinfeld, J. H., Shilling, J., Smith, J. N., Thornton, J. A., Volkamer, R., Wang, J.,

1034   Worsnop, D. R., Zaveri, R. A., Zelenyuk, A., and Zhang, Q.: Recent advances in

1035   understanding secondary organic aerosol: Implications for global climate forcing, Rev.

1036   Geophys., 55, 509–559, 2017.

1037 Shrivastava, M., Fast, J., Easter, R., Gustafson, W. I., Zaveri, R. A., Jimenez, J. L., Saide, P.,

1038   and Hodzic, A.: Modeling organic aerosols in a megacity: comparison of simple and

1039   complex representations of the volatility basis set approach, Atmos. Chem. Phys., 11,

1040   6639–6662, 2011.

1041 Sun, Y., Jiang, Q., Wang, Z., Fu, P., Li, J., Yang, T., and Yin, Y.: Investigation of the sources and

1042   evolution processes of severe haze pollution in Beijing in January 2013, J. Geophys. Res.,

1043   Atmos., 119, 4380–4398, 2014.

1044 Tang, J., Li, Y., Li, X., Jing, S., Huang, C., Zhu, J., Hu, Q., Wang, H., Lu, J., Lou, S., Rao, P.,

1045   and Huang, D.: Intermediate volatile organic compounds emissions from vehicles under

1046   real world conditions, Sci. Total Environ., 788, 147795, 2021.

1047   Tao, J., Zhang, L., Cao, J., and Zhang, R.: A review of current knowledge concerning $PM_{2.5}$

1048   chemical composition, aerosol optical properties and their relationships across China,

1049   Atmos. Chem. Phys., 17, 9485–9518, 2017.

1050   Tkacik, D. S., Presto, A. A., Donahue, N. M., and Robinson, A. L.: Secondary organic aerosol

1051   formation from intermediate-volatility organic compounds: Cyclic, linear, and branched

1052   alkanes, Environ. Sci. Technol., 46, 8773–8781, 2012.

1053   Tsimpidi, A. P., Karydis, V. A., Zavala, M., Lei, W., Molina, L., Ulbrich, I. M., Jimenez, J. L.,

1054   and Pandis, S. N.: Evaluation of the volatility basis-set approach for the simulation of

1055   organic aerosol formation in the Mexico City metropolitan area, Atmos. Chem. Phys., 10,

1056   525–546, 2010.

1057   US EPA: Final Report, SPECIATE Version 5.1, Database Development Documentation,

1058   available at: https://www.epa.gov/air-emissions-modeling/speciate-51-and-50-addendum-

1059   and-final-report (last access: 8 August 2021), 2021

1060   Woody, M. C., Baker, K. R., Hayes, P. L., Jimenez, J. L., Koo, B., and Pye, H. O. T.:

1061   Understanding sources of organic aerosol during CalNex-2010 using the CMAQ-VBS,

1062   Atmos. Chem. Phys., 16, 4081–4100, 2016.

1063   Wu, L., Ling, Z., Liu, H., Shao, M., Lu, S., Wu, L., and Wang, X.: A gridded emission inventory

1064   of semi-volatile and intermediate volatility organic compounds in China, Sci. Total

1065   Environ., 761, 143295, 2021.

1066   Wu, L., Wang, X., Lu, S., Shao, M., and Ling, Z.: Emission inventory of semi-volatile and

1067   intermediate-volatility organic compounds and their effects on secondary organic aerosol

1068   over the Pearl River Delta region, Atmos. Chem. Phys., 19, 8141–8161, 2019.

1069   Xu, L., Guo, H., Boyd, C. M., Klein, M., Bougiatioti, A., Cerully, K. M., Hite, J. R., Isaacman-

1070   VanWertze, G., Kreisberg, N. M., Knote, C., Olson, K., Koss, A., Goldstein, A. H., Hering,

1071   S. V., de Gouw, J., Baumann, K., Lee, S., Nenes, A., Weber, R. J., and Ng, N. L.: Effects

1072   of anthropogenic emissions on aerosol formation from isoprene and monoterpenes in the

1073   southeastern United States, P. Natl. Acad. Sci. USA, 112, 37–42, 2015.

1074   Yang, W., Li, J., Wang, W., Li, J., Ge, M., Sun, Y., Chen, X., Ge, B., Tong, S., Wang, Q., and

1075   Wang, Z.: Investigating secondary organic aerosol formation pathways in China during

1076   2014, Atmos. Environ., 213, 133–147, 2019.

1077   Yao, T., Li, Y., Gao, J., Fung, J. C. H., Wang, S., Li, Y., Chan, C. K., and Lau, A. K. H.: Source

1078   apportionment of secondary organic aerosols in the Pearl River Delta region: Contribution

1079   from the oxidation of semi-volatile and intermediate volatility primary organic aerosols,

1080   Atmos. Environ., 222, 117111, 2020.

1081   Yu, K., Zhu, Q., Du, K., and Huang, X.: Characterization of nighttime formation of particulate

1082   organic nitrates based on high-resolution aerosol mass spectrometry in an urban

1083   atmosphere in China, Atmos. Chem. Phys., 19, 5235–5249, 2019.

1084   Yuan, B., Shao, M., Lu, S., and Wang, B.: Source profiles of volatile organic compounds

1085   associated with solvent use in Beijing, China, Atmos. Environ., 44, 1919–1926, 2010.

1086   Zhang, H, Yee, L. D., Lee, B. H., Curtis, M. P., Worton, D. R., Isaacman-VanWertz, G.,

1087   Offenberg, J. H., Lewandowski, M., Kleindienst, T. E., Beaver, M. R., Holder, A. L.,

1088   Lonneman, W. A., Docherty, K. S., Jaoui, M., Pye, H. T. O., Hu, W., Day, D. A.,

1089   Campuzano-Jost, P., Jimenez, J. L., Guo, H., Weber, R. J., de Gouw, J., Koss, A. R.,

1090   Edgerton, E. S., Brune, W., Mohr, C., Lopez-Hilfiker, F. D., Lutz, A., Kreisberg, N. M.,

1091   Spielman, S. R., Hering, S. V., Wilson, K. R., Thornton, J. A., and Goldstein, A. H.:

1092   Monoterpenes are the largest source of summertime organic aerosol in the southeastern

1093   United States, P. Natl. Acad. Sci. USA, 115, 2038–2043, 2018.

1094   Zhang, Q., Jimenez, J. L., Canagaratna, M. R., Allan, J. D., Coe, H., Ulbrich, I., Alfarra, M. R.,

1095   Takami, A., Middlebrook, A. M., Sun, Y. L., Dzepina, K., Dunlea, E., Docherty, K.,

1096   DeCarlo, P. F., Salcedo, D., Onasch, T., Jayne, J. T., Miyoshi, T., Shimono, A., Hatakeyama,

1097   S., Takegawa, N., Kondo, Y., Schneider, J., Drewnick, F., Borrmann, S., Weimer, S.,

1098   Demerjian, K., Williams, P., Bower, K., Bahreini, R., Cottrell, L., Griffin, R. J., Rautiainen,

1099   J., Sun, J. Y., Zhang, Y. M., and Worsnop, D. R.: Ubiquity and dominance of oxygenated

1100   species in organic aerosols in anthropogenically-influenced Northern Hemisphere

1101   midlatitudes, Geophys. Res. Lett., 34, L13801, 2007.

1102   Zhang, Q., Jimenez, J. L., Canagaratna, M. R., Ulbrich, I. M., Ng, N. L., Worsnop, D. R., and

1103   Sun, Y.: Understanding atmospheric organic aerosols via factor analysis of aerosol mass

1104   spectrometry: a review, Anal. Bioanal. Chem., 401, 3045−3067, 2011.

1105   Zhang, Y., Vijayaraghavan, K., and Seigneur, C.: Evaluation of three probing techniques in a

1106   three-dimensional air quality model, J. Geophys. Res., Atmos., 110, D02305, 2005.

1107   Zhao, B., Wang, S., Donahue, N. M., Jathar, S. H., Huang, X. F., Wu, W., Hao, J., and Robinson,

1108   A. L.: Quantifying the effect of organic aerosol aging and intermediate-volatility emissions

1109   on regional scale aerosol pollution in China, Sci. Rep., 6, 28815, 2016a.

1110   Zhao, Y., Hennigan, C. J., May, A. A., Tkacik, D. S., De Gouw, J. A., Gilman, J. B., Kuster, W.

1111   C., Borbon, A., and Robinson, A. L.: Intermediate-volatility organic compounds: A large

1112   source of secondary organic aerosol, Environ. Sci. Technol., 48, 13743–13750, 2014.

1113   Zhao, Y., Kreisberg, N. M., Worton, D. R., Isaacman, G., Weber, R. J., Liu, S., Day, D. A.,

1114   Russell, L. M., Markovic, M. Z., VandenBoer, T. C., Murphy, J. G., Hering, S. V., and

1115   Goldstein, A. H.: Insights into secondary organic aerosol formation mechanisms from

1116   measured gas/particle partitioning of specific organic tracer compounds, Environ. Sci.

1117   Technol., 47, 3781−3787, 2013.

1118   Zhao, Y., Nguyen, N. T., Presto, A. A., Hennigan, C. J., May, A. A., and Robinson, A. L.:

1119   Intermediate volatility organic compound emissions from on-road diesel vehicles:

1120   Chemical composition, emission Factors, and estimated secondary organic aerosol

1121   production, Environ. Sci. Technol., 49, 11516–11526, 2015.

1122   Zhao, Y., Nguyen, N. T., Presto, A. A., Hennigan, C. J., May, A. A., and Robinson, A. L.:

1123   Intermediate Volatility Organic Compound Emissions from On-Road Gasoline Vehicles

1124   and Small Off-Road Gasoline Engines, Environ. Sci. Technol., 50, 4554–4563, 2016b.

1125   Zheng, M., Cass, G. R., Schauer, J. J., and Edgerton, E. S.: Source Apportionment of $PM_{2.5}$ in

1126   the Southeastern United States Using Solvent-Extractable Organic Compounds as Tracers,

1127   Environ. Sci. Technol., 36, 2361−2371, 2002.

1128   Zhu, S., Wang, Q., Qiao, L., Zhou, M., Wang, S., Lou, S., Huang, D., Wang, Q., Jing, S., Wang,

1129   H., Chen, C., Huang, C., and Yu, J. Z.: Tracer-based characterization of source variations

1130   of $PM_{2.5}$ and organic carbon in Shanghai influenced by the COVID-19 lockdown, Faraday

1131   Discuss., 226, 112, 2021.

1132 Zhu, W., Zhou, M., Cheng, Z., Yan, N., Huang, C., Qiao, L., Wang, H., Liu, Y., Lou, S., and

1133   Guo, S.: Seasonal variation of aerosol compositions in Shanghai, China: Insights from

1134   particle aerosol mass spectrometer observations, Sci. Total Environ., 771, 144948, 2021.

1135